Surround Suppression in Primate V1

H. E. JONES, K. L. GRIEVE, W. WANG, AND A. M. SILLITO
Department of Visual Science, Institute of Ophthalmology, University College London, London EC1V 9EL, United Kingdom

Received 26 May 2000; accepted in final form 20 April 2001

Jones, H. E., K. L. Grieve, W. Wang, and A. M. Sillito. Surround suppression in primate V1. *J Neurophysiol* 86: 2011–2028, 2001. We investigated the spatial organization of surround suppression in primate primary visual cortex (V1). We utilized drifting stimuli, configured to extend either from within the classical receptive field (CRF) to surrounding visual space, or from surrounding visual space into the CRF or subdivided to generate direction contrast, to make a detailed examination of the strength, spatial organization, direction dependence, mechanisms, and laminar distribution of surround suppression. Most cells (99/105, 94%) through all cortical layers, exhibited suppression (mean reduction 67%) to uniform stimuli exceeding the CRF, and 43% exhibited a more than 70% reduction. Testing with an annulus revealed two different patterns of surround influence. Some cells (37% of cells), classical surround suppression (CSS) cells exhibited responses to an annulus encroaching on the CRF that were less than the plateau in the spatial summation curve. The majority (63%), center-gated surround suppression (CGSS) cells, showed responses to annuli that equaled or exceeded the plateau in the spatial summation curve. Analysis suggested the CSS mechanism was implemented in all cells while the CGSS mechanism was implemented in varying strength across the sample with the extreme reflected in cells that gave larger responses to annuli than to a center stimulus. Reversing the direction of motion of the portion of the stimulus surrounding the CRF revealed four different patterns of effect: no reduction in the degree of suppression (22% of cells), a reduction in surround suppression (41%), a facilitation of the response above the level to the inner stimulus alone (37%), and a facilitation of the response above that to the inner stimulus alone that also exceeded the values associated with an optimal inner stimulus. The facilitatory effects were only seen for reverse direction interfaces between the central and surrounding stimulus at diameters equal to or more than the CRF size. The zones driving the suppressive influences and the direction contrast facilitation were often spatially heterogeneous and for a number of cells bore strong comparison with the class of behavior reported for surround mechanisms in MT. This suggests a potential role, for example, in extracting information about motion contrast in the representation of the three dimensional structure of moving objects.

INTRODUCTION

A number of studies have identified suppressive influences that reduce the responses of neurons in primate V1 when areas of visual space surrounding the classical receptive field are stimulated (Born and Tootell 1991; Kapadia et al. 1999; Knierim and Van Essen 1992; Nothdurft et al. 1999; Sceniak et al. 1999; Sillito et al. 1995). Some have reported these surround influences to be restricted to cells in the upper layers of V1 only (Born and Tootell 1991), although a recent study of the effect of contrast on spatial summation in V1 neurons (Sceniak et al. 1999) would suggest that common mechanisms may apply through all cortical layers. Indeed this latter study suggests that surround effects can be explained in terms of a difference of Gaussians model with overlapping Gaussians for the inhibitory and excitatory fields centered on the same point. In this sense, the mechanism underlying surround suppression would be an integrated component of the classical receptive field, and terms such as center and surround mechanisms become rather misleading. However, it seems likely that several mechanisms would have to underlie both the excitatory and the inhibitory Gaussians, and their interaction may not be linear and may depend on the spatial organization of the stimulus. For example, a layer 4 cell would receive direct thalamic input and horizontally linked intracortical excitatory connections together with inputs from cells in the underlying layer 6 (Ahmed et al. 1994; Callaway 1998; Ferster and Lindstrom 1985a,b; Peters et al. 1994). Present evidence suggests the synaptic efficacy of these different components of the excitatory input could be quite different (Ferster and Lindstrom 1985a,b; Stratford et al. 1996). Likewise a range of inhibitory processes will provide both a direct influence on individual cells and an indirect effect via their influence on the cells driving the intra-cortical facilitation. The potential dynamic complexity of these interactions is underlined by the work of Kapadia et al. (1995, 1999) in primates. Experiments in area MT have also reported suppressive surrounds of varying degrees of complexity with an organization that may encompass local to local motion comparisons and the extraction of complex features of the visual environment (Raiguel et al. 1995; Xiao et al. 1995, 1997a,b). This raises the possibility of a complexity to the organization of surround mechanisms in V1 that go beyond that predicted from an overlapping Gaussians model. In particular, the feedback from MT to V1 raises the possibility of complex motion-dependent effects drawing on the influence of MT. Thus following from our earlier report of surround driven suppressive and facilitatory effects in primate V1 (Sillito et al. 1995), we have utilized drifting stimuli to make a detailed examination of the strength, spatial organization, direction dependence, and laminar distribution of surround suppression in an attempt to further characterize the way in which it is implemented. The stimuli we have used here were all effective in driving MT cells (in some of these experiments we made simultaneous recordings in MT) (H. E. Jones, W. Wang, T. E. Salt, and A. M. Sillito, unpublished data)

Address for reprint requests: H. E. Jones, Dept. of Visual Science, Institute of Ophthalmology, University College London, Bath Street, London EC1V 9EL, UK (E-mail: h.jones@ucl.ac.uk).

The costs of publication of this article were defrayed in part by the payment of page charges. The article must therefore be hereby marked "*advertisement*" in accordance with 18 U.S.C. Section 1734 solely to indicate this fact.

and also enabled comparison with a number of other studies in MT and cat and primate V1. Our data here suggest a much stronger influence of surround suppression through all laminae than hitherto reported in primate V1, clear dependency on the relative direction of motion for the surround stimulus and two distinct patterns of bias to the spatial organization underlying the suppressive mechanisms. These observations are discussed in the context of the insight they suggest into the processing mechanisms pertaining in V1.

METHODS

Subjects

The experiments were carried out on 14 adult *Macaca mulatta* monkeys. The animals were treated according to the published guidelines on the use of animals in research (European Communities Council Directive 86/609/EEC) and the National Institutes of Health guidelines for the use of laboratory animals.

Animal preparation

Animals were initially premedicated with atropine sulfate (0.04 mg/kg im) and acepromazine maleate (0.05 mg/kg im). Anesthesia was induced with intramuscular injection of ketamine (10–15 mg/kg). Surgical procedures were carried out under ketamine anesthesia, and a solution of bupivicaine hydrochloride (0.75% wt/vol) was applied to all wound margins. After cannulation of the saphenous veins and trachea, the animal was transferred to a stereotactic frame. The ear bars of the stereotactic apparatus were coated with lignocaine hydrochloride gel. The dura overlying V1 was exposed via a craniotomy. Anesthesia was maintained throughout the course of the experiment either with halothane (0.1–0.4%) or sufentanil ($4–8\ \mu g \cdot kg^{-1} \cdot h^{-1}$) and a mixture of 70% N_2O and 30% O_2. End-tidal CO_2 levels, the electrocardiogram (ECG) waveform, intersystolic interval, and the frequency of spindles in the electroencephalogram (EEG) waveform were monitored at all times through the experiment. The rate and depth of artificial ventilation was adjusted to maintain end-tidal CO_2 at 3.8–4.2%; after completion of all surgical procedures, the level of anesthetic agent was adjusted to give a state of light anesthesia. Once a stable state was reached, any variation in the monitored parameters (change in the frequency of spindles, fall or fluctuation in intersystolic interval, rise in end-tidal CO_2) commensurate with a change in the depth of anesthesia was immediately compensated for by an increase in the level of anesthetic reagent. Following completion of all surgical procedures and after a stable state of anesthesia had been established, animals were immobilized with an infusion of vecuronium bromide ($0.1\ mg \cdot kg^{-1} \cdot h^{-1}$) in glucose-enriched lactated Ringer solution. Temperature was maintained at 38°C by use of a thermostatically controlled electric heating blanket. All wound margins were dusted with topical application of Neomycin sulfate and Noricillin [procaine penicillin (15 mg/kg) and benzathine penicillin (11.25 mg/kg)im] was administered daily. Dexamethasone (1 mg/kg iv) was administered daily to reduce cerebral edema.

The pupils were dilated and accommodation paralyzed with topical application of atropine methonitrate (2% wt/vol). The eyes were protected with gas permeable contact lenses, and brought to focus on a semi-opaque tangent screen/front surface mirror at a distance of 0.57 or 1 m, using supplementary lenses and 2-mm diam artificial pupils. The locations of the blind spot and fovea were located and plotted using a reversible ophthalmoscope.

Apparatus

Single-unit activity was recorded from area V1 using arrays of tungsten in glass microelectrodes (Merrill and Ainsworth 1972). Electrode penetrations were angled to avoid recording from locations underlying the array entry point. Data were collected and visual stimuli generated using the Cambridge Electronic Design (Cambridge, UK) VS system in conjunction with a Picasso Image Generator (John Daughman, USA), presented on a Tektronix 608 tube. For further details, refer to Sillito et al. (1993). Spikes were stored with a 0.1-ms interval resolution and could subsequently be processed with respect to any aspect of the stimulus variables used during data collection. We first identified and hand mapped receptive fields using an overhead projector and the tangent screen of a plotting table. Once the receptive fields had been characterized in this way, we introduced a 45° front-surfaced mirror into the light path, deflecting the animal's plane of vision to a vertically mounted, 608 Tektronix tube at a distance of 0.57 or 1 m for controlled presentation of visual stimuli. The 608 tube was mounted on a cradle that could be shifted over a set of floor mounted tracks and tracks mounted in a slave carrier to roughly center the display on one of the receptive fields. We utilized the alignment of the receptive field on the tangent screen and 45° beam splitter to achieve this. We could fine tune the centering of the receptive field on the 608 tube using micrometer adjustments on the carrier mechanisms and software adjustment of the display center. These adjustments were checked with reference to the magnitude of the responses generated either by small flashing spots or small patches of an optimally oriented drifting sinusoidal grating presented in a range of spatial locations forming a sequential grid over the field. Accurate centering of the display over the receptive fields studied was critical to our experiments, and so the fine tuning of the centering was a standardized procedure for every cell and was checked throughout data gathering sequences.

Visual stimuli

For the preliminary evaluation of cell response properties, we used simple visual stimuli comprising flashing spots, drifting bars, and patches and annuli of drifting sinusoidal gratings. Parameters such as spatial frequency, temporal frequency, orientation, and bar length or spot/patch diameter were varied in a randomly interleaved sequence. A blank stimulus was included in each block for the assessment of spontaneous activity levels. The contrasts $(L_{max} - L_{min})/(L_{max} + L_{min})$ routinely used were in the range 0.1–0.36 with a mean luminance of 14 cd m^{-2}. To explore the effects of direction contrast on patch suppression, we used concentric bipartite sinusoidal gratings centered over the receptive field. We kept the contrast, spatial frequency, and drift rate constant in both inner and outer stimuli but varied the direction of drift of the inner and outer stimuli. The phase of our inner and outer displays were locked together with reference to the center of the display so that for concentric stimuli, when the direction of drift of both components was the same, they appeared as a single grating. Central patch size and inner diameter of the outer field ranged between 0.3 and 6.0°. Spatial frequency was in the range 1–4 cycles/° (cpd) and drift rate was 1.0–4.0 Hz. All tests were done with monocular visual stimulation of the cell's dominant eye.

To examine the spatial location of suppressive zones, we used two square patches of optimally oriented sinusoidal grating. The gratings drifted within each patch, and spatial frequency, direction of motion, and drift rate were kept constant in both patches. One grating patch (the notional inner stimulus) was centered over the CRF while the second stimulus patch was presented in randomized sequence at a range of locations around the field. Central and outer patch sizes ranged from 0.5 to 2°. For some cells, we also explored the effect of reversing the direction of drift of the grating in the second patch.

Experimental protocol and analysis

PRELIMINARY EVALUATION OF RECEPTIVE FIELDS. Isolated single units were classified as simple or complex according to conventional criteria (Hubel and Wiesel 1962; Skottun et al. 1991). After the receptive field center had been localized as described in the preceding

text, we quantitatively checked preferred orientation and direction of motion using a patch of sinusoidal grating localized over the receptive field center with orientation and direction of drift varied in a randomized and interleaved sequence.

MAPPING THE CLASSICAL RECEPTIVE FIELD. Because of the way the mechanisms driving center and surround mediated influences overlap in primate V1, it is difficult to define what is precisely meant by the term classical receptive field. It might be taken to include the spatial borders of the processes driving surround effects, but these are often difficult to define. Equally the area of visual space from which excitatory responses can be obtained may not define the extent of the excitatory mechanism or excitatory field because the underlying inhibitory mechanism may suppress the weaker excitatory influences. In this study, we have used the term classical receptive field, CRF, to indicate the area of visual space from which excitatory responses, as judged by the spiking activity of the cell, could be obtained. The precise measurement is influenced by the procedure used to map the field.

We determined the precise location and spatial extent of the CRF using four procedures and took the value for the CRF size from the procedure giving the largest measurement. This avoided the potential danger of underestimating the size of the CRF (Sengpiel et al. 1997; Walker et al. 2000). First, we explored the spatial distribution of locations from which a contrast modulated patch or a patch of optimally oriented drifting grating elicited responses (we termed this the XY patch method). A variety of patch sizes from 0.2 to1.0° were used for this test. They were presented in a randomized sequence over a set of spatial locations defined in rectangular coordinates. The location giving the largest response was used to define the CRF center, and the coordinates of our display were adjusted to match CRF center and display center. This involved several iterations with variations of patch size and display coordinates to optimize both centering and assessment of CRF dimensions. The data from all the test runs in these procedures were stored. We also assessed the dimensions of the receptive field with a drifting bar stimulus to quantify the *xy* coordinates defining the width and length of the area from which a bar would drive excitatory responses. Next, we examined the effect of increasing the diameter of an optimally oriented patch of grating centered over the receptive field center. This was followed by a similar test but with an annulus of optimally oriented grating with its virtual center over the center of the CRF, and the variable was the diameter of the inner wall of the annulus. This latter test brought an optimally oriented border in toward the receptive field center. The stimulus variables for all the protocols used to assess RF size were randomized and interleaved and responses assessed from the mean computed from 10 to 50 presentations of the stimulus. The data from the four methods gave similar values, but those from the XY patch and bars were the smallest. Across the sample ($n = 105$), the mean value for CRF size derived from the XY patch method was $0.9 \pm 0.08°$ (mean $\pm$ SE) compared with 0.75 ± 0.10 from the bars, $1.1 \pm 0.14°$ from the optimal summation diameter and $1.15 \pm 0.17°$ derived from the annulus paradigm. In all but two cases, the values used for defining the CRF borders were drawn from either the optimal summation diameter or annulus paradigm, with the two exceptions following from cases where the XY patch test revealed the largest values.

To minimize any effects of adaptation by persistent presentation of a stimulus at the cell's optimal orientation and to generate control data for subsequent tests, the protocols varying patch diameter or annulus inner wall diameter also varied the orientation of the stimulus in a randomized interleaved fashion. The values for the optimal orientation were then extracted from the data sets and used to plot the patch tuning curves.

QUANTIFYING RESPONSES. Responses were computed from the mean firing rate averaged over the full number of stimulus presentations. Typically we presented three to five stimulus cycles of each stimulus condition repeated over 5–20 trials. For each cell, we calculated a patch suppression index (PSI) according to the formula $\text{PSI} = [1 - (R_{\text{plat}}/R_{\text{opt}})]*100$, where R_{opt} and R_{plat} denote the responses elicited by the optimal and plateau stimuli, respectively. Thus cells showing no suppression to large diameter stimuli would have a PSI of 0, while those showing total response suppression would have a PSI of 100. To explore the effects of direction contrast on patch suppression, we used concentric bipartite sinusoidal gratings centered over the receptive field and varied the direction of drift of the inner and outer stimuli. Cells were regarded as showing no direction contrast if the response to the inner stimulus drifting in the preferred direction in the presence of an outer stimulus drifting in the reverse direction was not significantly different to the response observed when the inner and outer stimuli both drifted in the same direction ($P = >0.05$, paired *t*-test). Cells were regarded as showing direction contrast modulation if the response to the reverse direction configuration was significantly larger ($P < 0.05$) than the response observed when the inner and outer stimuli both drifted in the preferred direction [thus "direction contrast modulation" is analogous to the term "orientation contrast" (Knierim and Van Essen 1992)]. In some cases, the response to the direction contrast stimulus configuration exceeded the response to the inner stimulus presented alone ("direction contrast facilitation"). To quantify this, we calculated the percentage response increase elicited by the reverse direction configuration with respect to the response level elicited by the inner patch of grating presented alone. Cells were only regarded as showing direction contrast facilitation if the response to the reverse direction configuration was significantly larger ($P < 0.05$) than the responses to the same direction configuration and the inner stimulus alone and exceeded that to the inner alone by 10% or more. (We observed one example where the response to the reverse direction configuration was significantly smaller than the response to the same direction configuration. For simplicity, this cell was included in the no direction contrast grouping.)

Contour maps of the CRF were plotted as a function of stimulus position on a ten level iso-response contour plot [where the distance between contours was defined by the equation $(R_{\max} - R_{\min})/1 +$ number of levels, and the first level was defined by $R_{\min}$], using a spline fitting algorithm for interpolation between recorded positions.

To examine the spatial location of suppressive zones, we used two square patches of optimally oriented sinusoidal grating. One grating patch was centered over the CRF while the second stimulus patch was presented in randomized sequence at a range of locations around the field. For graphical representation of this data, we constructed three-dimensional surface maps documenting the modulatory effect of the second stimulus on the response to the simultaneously presented central stimulus at a range of *xy* locations. The data were represented as iso-response surface plots, using a spline fitting algorithm for interpolation between recorded locations. The central point in these surfaces always represented the response to the central stimulus presented alone. The data were also represented as two-dimensional iso-response contour maps (shown beneath each surface plot). We adopted the procedures and criteria used in area MT by Xiao et al. (1997b) to quantify the angular distribution of the suppressive zones. First, we computed the strength of suppression (expressed as a percentage of the response to the center stimulus alone) for each surround stimulus location, according to the formula $S = [1 - (R_{cs}/R_c)]*100$, where S is the strength of the antagonistic surround elicited by a particular surround stimulus location, R_{cs} is the response to the combination of the center and surround stimulus, and R_c is the response to the center stimulus presented alone. We then computed two selectivity indices (SIs) from the level of surround antagonism generated by each of the surround stimulus positions using a formula, based on circular statistics, for calculating the length of the mean vector

$$\text{SI} = \frac{\sqrt{\left[\sum_{i=1}^{n} Si \cdot \sin(\alpha i)\right]^2 + \left[\sum_{i=1}^{n} Si \cdot \cos(\alpha i)\right]^2}}{\sum_{i=1}^{n} Si}$$

where *Si* is the magnitude of the surround suppression at each surround location, αi. Following Xiao et al. (1997b), we termed the first of the two SIs the unimodal selectivity index (USI), which was calculated from the actual αi values. The USI is a measure of the degree of unimodality of the surround antagonism, i.e., the tendency for the surround antagonism to be concentrated in one location. A USI value of 1.0 indicates that only a single surround position was effective in modulating activity, whereas a value of 0.0 denotes a uniform angular distribution of surround antagonism. The second SI, the bimodal selectivity index (BSI), was calculated with each αi value doubled and reflects the degree of bimodal distribution, or the tendency for surround antagonism to be concentrated along an axis, on opposite sides of the CRF. A BSI value of 1.0 indicates that all suppression originates along a single axis, whereas a values of 0.0 denotes that the suppression along each axis is equal.

The Rayleigh test (Batschelet 1981), which tests the hypothesis that the data are uniformly distributed, and the USI and BSI values were employed for classifying the angular distribution of the antagonistic surround into three classes: uniform or circularly symmetric surround suppression (Rayleigh test $P \geq 0.05$), asymmetric surround suppression (Rayleigh test $P < 0.05$ and USI $>$ BSI) and bilaterally symmetric suppression (Rayleigh test $P < 0.05$ and BSI $>$ USI).

To quantify the surround location showing most suppression, we computed the optimal angle (OPA) for each cell using the formula for calculating the mean vector angle (Batschelet 1981)

$$\mathrm{OPA} = \arctan\left[\frac{\sum_{i=1}^{n} Si \cdot \sin(\alpha i)}{\sum_{i=1}^{n} Si \cdot \cos(\alpha i)}\right]$$

For cells with a bilaterally symmetric surround, the OPA represents the angle of the axis through the two optimal surround locations.

RECONSTRUCTION OF RECORDING SITES. At the end of each electrode penetration, key recording sites were marked by electrolytic lesions (3–5 μA for 3–5 s, electrode negative). At the conclusion of the experiment, animals were overdosed with pentobarbital sodium, desanguinated with phosphate-buffered saline (PBS), and perfused with paraformaldehyde followed by sucrose in PBS. Frozen sections were cut at 40 μ, and alternate sections were stained by the Nissl method and an enhanced cytochrome oxidase method, respectively. Sections containing electrolytic lesions were drawn at low power. Adjacent sections were aligned precisely using blood vessels and section outlines as reference points.

RESULTS

The results reported here derive from 105 cells recorded in layers 2–6 of primate V1 at eccentricities from 2–6°. Our sample comprised 61 S type cells and 44 C type cells. All the effects reported applied equally to both S and C types.

Spatial summation curves and suppression

For all the cells in our sample (105), we determined the change in response as the diameter of a patch of optimally oriented drifting grating was varied. The core procedures we used to center on the CRF, map its size, and examine its spatial summation characteristics are illustrated in Fig. 1 for a layer 5 cell. The histogram (Fig. 1*A*) shows the response of the cell to an optimally oriented 0.3° square of drifting grating presented in a randomized sequence at a range of locations over and around the receptive field. The responsive regions are clearly defined. The contour plot (Fig. 1*B*) provides an overview of the shape of the field as determined by this method. The spatial summation curve (Fig. 1*C*) shows the response of the cell to

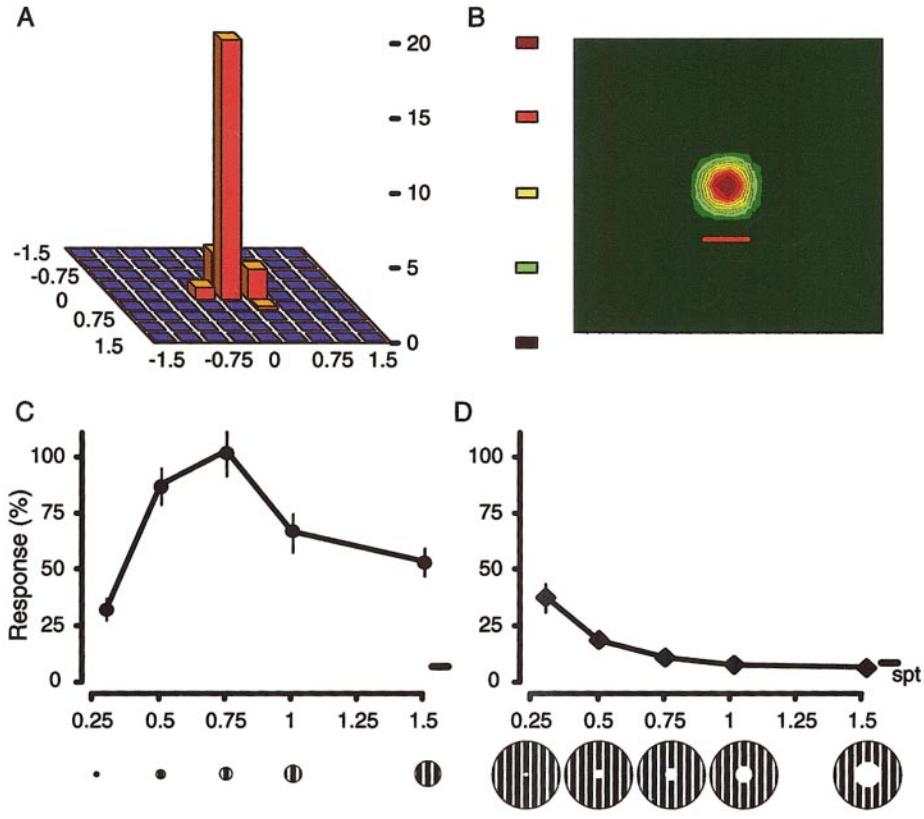

FIG. 1. Classical receptive field and spatial summation properties. *A*: the 3-dimensional (3-D) histogram documents the response to a small patch of an optimally oriented, drifting sinusoidal grating presented at a range of spatial locations spanning a $3 \times 3°$ area of visual space encompassing the cell's receptive field location. Responses (computed from the mean response rate averaged from the full stimulus cycle over 15 stimulus repeats) were elicited only from a very circumscribed area of visual space. [Patch diameter, 0.3°. Spatial frequency (SF), 2 cycles/degree (cpd). Temporal frequency (TF), 3 Hz. Contrast 0.36. Vertical scale denotes response in imp/s. C type layer 5 cell.] *B*: contour plot delineating the shape of the receptive field shown in *A*. The magnitude of the cell's response is shown by the shading of the contours as denoted by the color scale to the *left*. The scale bar shown in red denotes 0.5°. See METHODS for further details. *C*: the tuning curve plots the variation in response magnitude for increasing diameters of an optimally oriented patch of grating centered over the receptive field center. Responses were normalized to the response value elicited by the optimal diameter patch (9 imp/s). Error bars indicate ±1 SE. Black line to the right denotes spontaneous activity level. The patch suppression index for this cell (see METHODS) was 43%. Stimulus details as in *A* but 50 stimulus repeats. *D*: the tuning curve documents the response to varying the inner diameter of an annulus of optimally oriented grating. Responses were normalized to the maximal response seen in the patch tuning curve (*C*). Stimulus details as in *C*.

varying the diameter of an optimally oriented patch of drifting grating. The response rose and then fell as the stimulus reached and then exceeded 0.75° in diameter, suggesting a potent suppressive or disfacilitatory influence beyond this point. This spatial summation curve was typical of the majority of cells we saw in primate V1. In addition to quantifying the response to varying the diameter of a circular patch, we also plotted the response to varying the diameter of the inner wall of an annulus of drifting grating. This provided a mirror image probe to the sequence of patch diameters and enabled us to assess the response of the cell to stimulation of outer regions of the receptive field in the absence of stimulation of the central region. The *bottom right curve* shows the response to varying the diameter of the inner wall of an optimally oriented annulus of drifting grating. This started to exert a small excitatory effect at 0.75°. For the sake of simplicity, we have used the term CRF here to indicate the area of visual space from which the cell showed clear excitatory responses with the tests used. In the case of the example shown in Fig. 1, we defined this as 0.75°.

We show two further examples of spatial summation curves for a circular patch of drifting grating in Fig. 2, *A* and *B*. The variation in patch suppression over our cell sample is shown by the histogram in Fig. 2*C*. Here we have quantified the degree of suppression in terms of the percentage reduction in the response observed at the plateau of the spatial summation curve elicited by larger diameter stimuli in comparison to the response seen to an optimal diameter patch (see METHODS). The percentage reduction in response is represented in steps along the abscissa and number of cells in each category on the ordinate. The majority of the cells (99/105, 94%) exhibited response suppression to large diameter stimuli with a mean suppression of 67% (±2.07%; mean ± SE). This decrement in response with increasing stimulus diameter was highly significant across the population ($P < 0.001$ Wilcoxon test) and reflected a potent reduction in the output of V1 cells for optimally oriented stimuli extending beyond the CRF. Indeed it is worth underlining the fact that 80% of the sample exhibited a more than 50% suppression and 43% a more than 70% suppression in response. We recognize two possible sources of error in these observations. The first was that in a few cases, we were unable to generate stimuli large enough to be sure that we had accessed the full extent of the surround suppression and the second that in a few cases, we were unable to generate stimuli small enough to be sure we had accessed the cell's optimal response. However, both these would cause us to underestimate the degree of surround suppression and so would emphasize rather than diminish the finding that the majority of primate V1 cells are strongly suppressed by stimuli extending beyond their CRF.

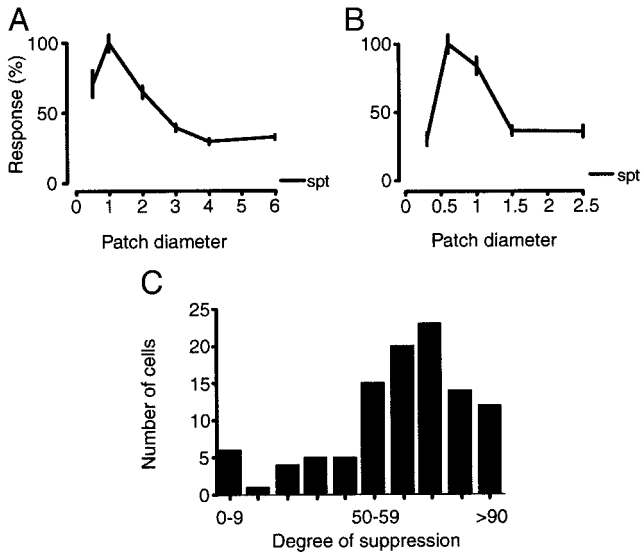

FIG. 2. Patch suppression across our V1 cell sample. *A* and *B*: 2 further examples of spatial summation curves. Conventions as for Fig. 1*C*. For *A*, the patch suppression index was 69% and the optimal response 167 imp/s. (30 stimulus repeats. SF, 2cpd; TF, 3 Hz; contrast, 0.36. C type layer 4B cell.) For *B*, PSI was 64% and optimal response 33 imp/s. (Further details as in *A*. S type layer 4Cα cell.) *C*: block histogram plotting the distribution of patch suppression across the V1 cell population ($n = 105$). Cells were subdivided into 10 categories of patch tuning, binned in 10% epochs. Thus cells in category 0–9% had little or no patch tuning, cells in category >90% showed little or no response to large diameter patches (see METHODS for details of quantification).

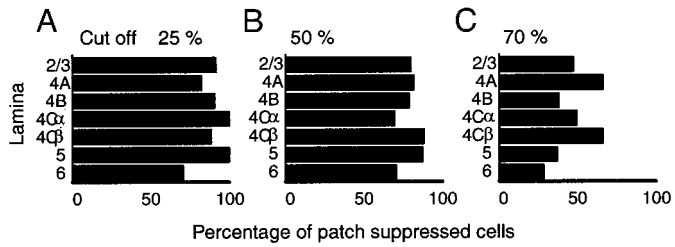

FIG. 3. Laminar distribution of patch-suppressed cells. Cortical layers were assigned according to the criteria of Lund (1988). The 3 block histograms show the percentage of patch suppressed cells in each lamina. For the histogram in *A*, any cell showing 25% or more suppression was regarded as patch suppressed. *B*: only cells showing 50% or more suppression were regarded as patch suppressed. *C*: cells were classed as patch suppressed only if the suppression with large diameter patches exceeded 70%. Regardless of the cutoff value chosen, patch suppressed cells were distributed across all laminae.

These observations might follow from a sample restricted to the superficial layers (cf. Born and Tootell 1991), or they might encompass a substantial laminar variation in the degree of patch suppression. Given the variation in connectivity of the different layers, it might be expected that cells in the different layers would show large variations in the degree of patch suppression. Interestingly, as shown in Figs. 3 and 4, we were unable to demonstrate a laminar variation in the distribution of

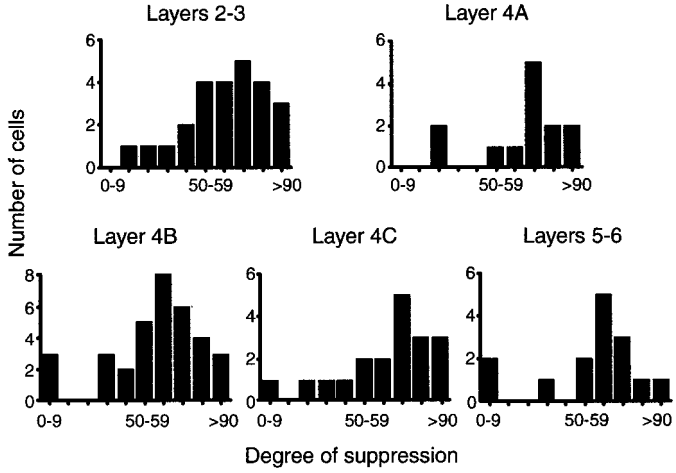

FIG. 4. Block histograms plot the distribution of patch suppression for different cortical layers (noted *above* each histogram). Cells were subdivided into ten categories of patch tuning, binned in 10% epochs as described in the legend to Fig. 2*C*.

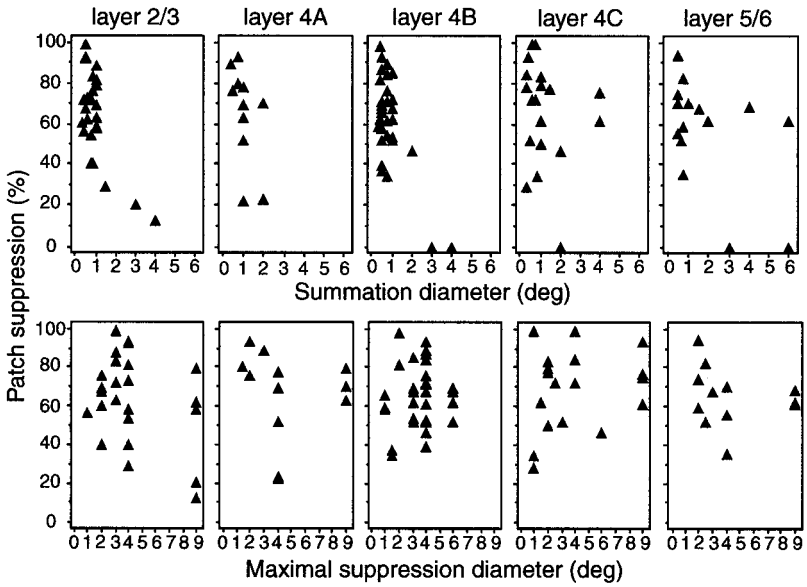

FIG. 5. The scatter diagrams plot the magnitude of patch suppression (%) vs. optimal summation diameter (*top row*) and vs. maximal suppression diameter (*bottom row*) for different cortical layers (noted *above* each plot).

cells showing surround suppression. The range of the indices of patch suppression was similar through all laminae. Figure 3, *A–C*, shows the laminar distribution of cells showing a more than 25, 50, and 70% reduction in response with stimulus diameter while Fig. 4 shows the number of cells in each lamina falling in the groups summarized in Fig. 2*C*. We also compared the distribution of optimal summation diameters and the distribution of stimulus diameters eliciting maximal suppressive effects across cortical layers. The scatter diagrams in Fig. 5 plot, for each lamina, the magnitude of patch suppression versus optimal summation diameter (*top*) and versus maximal suppression diameter (*bottom*). Again, there is little evidence to support any obvious differences across layers. In Table 1, we summarize, for each layer, the mean (±SE) values observed for patch suppression, optimal summation diameter, maximal suppressive diameter and spatial frequency used. Once more, there appears to be little laminar variation in the mean values observed for any of these parameters, although, interestingly, the optimal summation diameter for layer 5 and 6 cells was nearly double that seen for the other cortical layers. In general, the mechanism underlying patch suppression would appear to be common to all processing steps within V1 and possibly represents a general algorithm pertaining at this level in the system. The distribution of surround suppression through all layers of V1, plus the numbers of cells showing high levels of suppression, underlines the fact that extensive stimuli (4–9° diameter) will tend to minimize the output of a column. Furthermore, for eccentricities in the region of 5° as explored in the present work, even a 2° stimulus will result in substantive attenuation of the output of many cells in a column.

Dissection of the spatial organization of suppressive mechanisms

Generally, suppression in the receptive fields of cat V1 cells has been associated with either suppressive end zones, suppressive side bands, or both (DeAngelis et al. 1994; Hubel and Wiesel 1965; Kato et al. 1978; Orban et al. 1979a,b; Walker et al. 1999). It is important to know how the suppression we examined here with patches of varying diameter links to discretely identifiable end zones or side bands. Hence we included in our tests a protocol examining the influence of a second discrete patch of grating introduced at a stepped series of locations around a patch of rectangular drifting grating overlying the CRF. Examples of the data obtained from this are shown in Fig. 6, *A–J*. These surface plots show the variation in response magnitude to the stimulus overlying the CRF induced by the presentation of the second stimulus at any of the locations around the CRF (in a randomized interleaved sequence) as indicated by the matrix of points in the icon diagram above the records. The plots are all oriented so that the axis of the optimal orientation of the cell lies along the plane indicated in the icon diagram. In each case the center point of the records and the color, dark green, indicates the response level associated with the inner stimulus alone. All the cells in the examples *A–J* in Fig. 6 exhibited strong surround suppression with increase in the diameter of a circular patch of drifting grating. However, the detailed dissection of the zones around the CRF revealed patterns of influence that bore no relation to the degree of suppression following from an increase in the diameter of a circular patch of grating. The cell in Fig. 6*A* was not

TABLE 1. *Summary of spatial summation characteristics across cortical layers*

Layer	3	4A	4B	4C	5/6
Patch suppression, %	67 (5.31)	67 (6.67)	67 (2.91)	71 (5.23)	66 (4.00)
Summation diameter, deg	0.97 (0.17)	1 (0.15)	0.95 (0.14)	1.2 (0.25)	1.9 (0.51)
Maximal suppression diameter, deg	4.2 (0.51)	4.6 (0.31)	3.5 (0.26)	4 (0.50)	4.4 (0.76)
Spatial frequency, cpd	2.4 (0.10)	2.3 (0.22)	2.4 (0.09)	2.3 (0.17)	2.3 (0.17)
n	25	12	34	19	15

Values in parentheses denote SE.

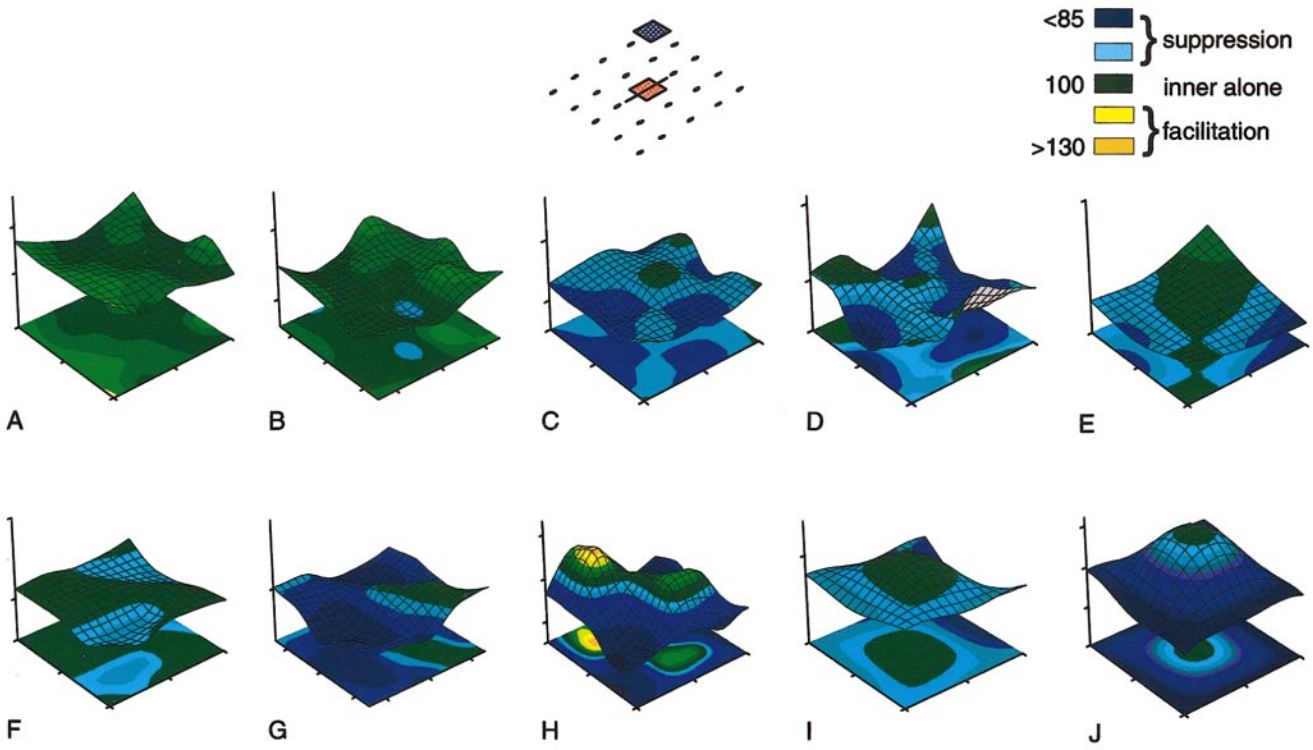

FIG. 6. Spatial organization of suppressive effects. The surface plots depict the modulatory effect of a 2nd stimulus presented at a range of spatial locations on the response to a central stimulus for 10 patch suppressed cells recorded in primate V1. The stimulus configuration comprised an inner stimulus (a square patch centered over the CRF containing an optimally oriented grating drifting in the cell's preferred direction of motion) and a 2nd stimulus (another square patch of optimally oriented grating drifting in the same direction of motion) that was positioned at a range of *xy* locations around the central stimulus (as depicted by the schematic diagram *above*). In each plot, the responses are normalized with respect to the response elicited by the center patch alone (100% in each case, dark green). Suppressive effects are denoted by blue colors, facilitatory effects by light green to yellow colors (see color scale bar *top right*). Center patch diameter ranged from 1 to 2° depending on each cell's CRF size. Spatial frequency ranged from 2 to 3 cpd. Temporal frequency, 3 Hz; contrast, 0.36.

suppressed by the second stimulus at any location around the CRF and that in Fig. 6*B* showed a slight suppression at one location only, while the cells in Fig. 6, *I* and *J*, were suppressed at all locations around the CRF. The other examples encompass patterns that show clear end zones and side bands (Fig. 6*C*) and those where suppressive effects partially surrounded the field or sat at either corner of the receptive field. The scatter diagram in Fig. 7 compares the amount of suppression observed at the plateau level of the patch summation curve to that observed using a discrete patch of grating positioned at the most effective surround location. As is clear, there was little correlation between the plateau level large diameter patch suppression and the most effective suppression elicited by a discrete patch. Indeed, for more than half the sample (58%), we were unable to detect any significant influence from side bands, end zones or corner zones (ANOVA) in cells showing significant patch suppression ($P < 0.05$ Wilcoxon test and ANOVA). Thus for these cells, a stimulus uniformly surrounding the CRF appeared to recruit otherwise subthreshold effects to exert a potent suppressive influence. Where there were clearly defined suppressive foci around the CRF, our data suggest a wide variety of configurations for their spatial organization. To quantify the degree of heterogeneity in these cells, we have used circular statistics (Batschelet 1981; Xiao et al. 1995, 1997b) to analyze the data. We used the criteria described by Xiao et al. (1997b) (see METHODS) to subdivide the cells into three groups, those exhibiting spatially uniform surround suppression, spatially asymmetric surround suppression, and bilaterally symmetric surround suppression. The majority of the cells analyzed in this way (81%) exhibited spatial heterogeneity of surround locations, although 19% showed spatially uniform surround suppression (an example is shown in Fig. 6*J*). Cells exhibiting heterogenous surrounds were

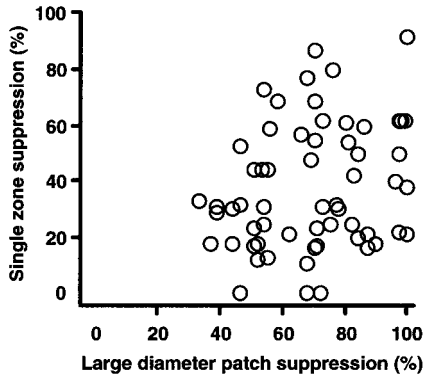

FIG. 7. Comparison of the amount of suppression observed at the plateau level of the patch summation curve to that observed using a discrete patch of grating positioned at the most effective surround location. The scatter diagram plots the degree of suppression (%) elicited by a large diameter patch along the *x* axis vs. the degree of suppression (%) elicited by the most effectively located discrete patch of grating along the *y* axis.

divided approximately equally into spatially asymmetric cells (44%) where the surround suppression was biased toward one location (e.g., Fig. 6*B*) and bilaterally symmetric cells (37%) where the surround effect was localized to two opposing regions along a single axis (e.g., Fig. 6*F*). For cells that exhibited spatially heterogenous surrounds, we asked whether the suppressive effects were localized to the ends, sides, or corners of the field. Interestingly, suppressive effects were nearly equally distributed in all directions round the CRF; there was no evidence to suggest that suppressive effects were concentrated in end-zone or side-band regions. As previously described, for 58% of cells showing significant patch suppression to a large grating patch, we were unable to detect any significant suppressive influence from a discrete second stimulus presented at any location around the CRF. Nonetheless, we also checked the degree of heterogeneity in the spatial organization of the surround for this subgroup of cells using the circular statistics method described in the preceding text. The results were essentially in accord with those for the 42% of cells that did show significant suppressive influences to a discrete second stimulus located at some position around the CRF. Thus the majority of cells showed heterogenous surrounds, and these were again divided approximately equally into spatially asymmetric and bilaterally symmetric types.

Dissection of surround effects with annuli

The spatial summation curves constructed from a circular patch of varying diameter reflect a situation where the receptive field center mechanism is always part of the integration driven by the stimulus. For this reason, we examined the effect of varying the diameter of the inner wall of an annulus of drifting grating so that we could explore the effect of a stimulus encroaching on the field from the surround without optimally activating the center mechanism. The data obtained revealed some interesting variances in the pattern of integration of surround influences and the mechanisms driving responses from the center of the CRF.

We explored these effects in detail for 54 cells in our sample by comparing the responses obtained in the patch tuning curves to effects elicited by annuli encroaching into the CRF but excluding the very center of the field. We grouped the data obtained with the annuli into three categories, those obtained with the inner border of the annulus in the outer 25% of the diameter of the CRF, those obtained with the annulus border in the middle 50%, and those obtained with the annulus border in the inner 25%. For the general comparisons, we have taken the category giving the largest response. Essentially these data highlighted the presence of cells with contrasting patterns of responses to the annuli. On the basis that an annulus by definition excludes the receptive field center, but encompasses all the surround, it is logical to expect that the best response to an annulus would be less than the plateau in the area summation curve. This indeed was the case for many cells (20/54, 37%). We separated out those cells showing responses lower than the plateau in the area summation curve using the criterion that the responses to the most effective annulus had to be significantly smaller than the plateau of the area summation curve ($P < 0.05$ level, *t*-test). For these cells, the mean response to the annulus was 61 ± 6.55% smaller than the value of the plateau in the patch tuning curve. Taking each category of the annulus encroachment within the CRF in turn the responses were 76 ± 6.41% smaller for the outer 25%, 64 ±

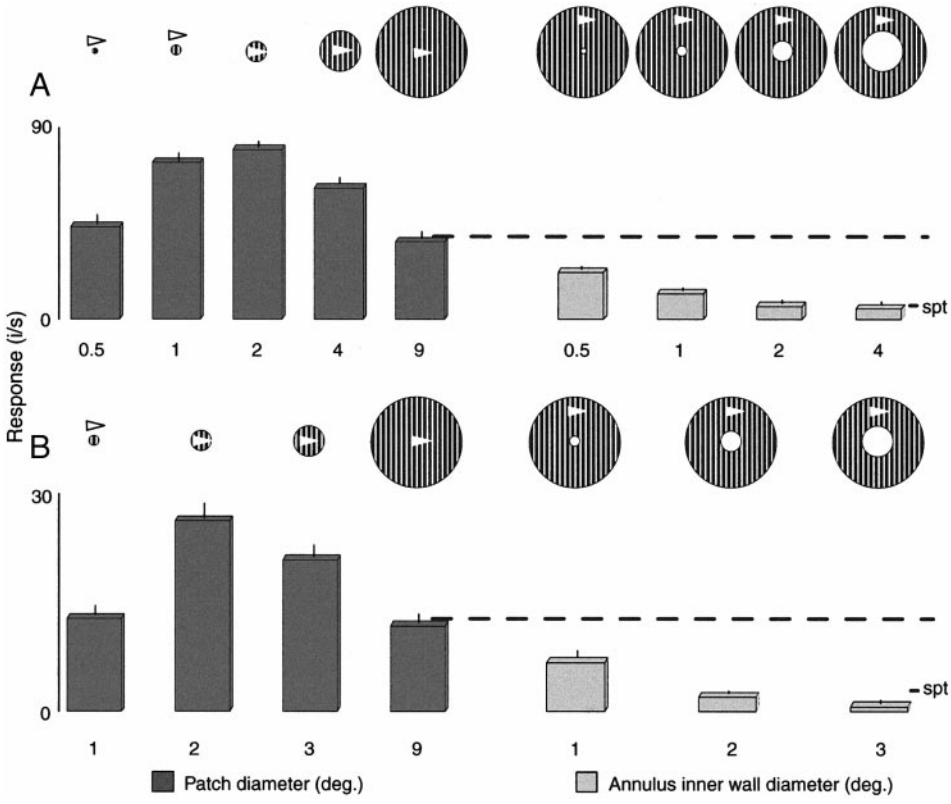

FIG. 8. Block histograms comparing the responses elicited by patches of varying diameter to those to annuli of a fixed outer diameter and a varying inner wall diameter. *A*: patch responses are denoted by the dark gray stippled bars to the *left* of the figure, annulus responses by the light gray stippled bars on the *right*. Stimulus configuration is denoted schematically *above* each bar. Patch and annulus inner wall diameters are indicated *below* each bar. The best response to an annulus (for an annulus with an inner wall diameter of 0.5°) was considerably smaller than the response elicited by the largest patch (response level denoted by dashed line). (50 stimulus repeats, SF, 2 c/d; TF, 3 Hz; contrast, 0.36. C type layer 4B cell.) *B*: stimulus conventions as in *A*. (Details as for *A*, but patch/annulus inner wall diameters are 1, 2, 3, and 9°. TF, 4 Hz; C type layer 3 cell.)

7.95% smaller for the middle category, and 68 ± 13.89% smaller for the inner category. Examples of the pattern of effect we saw are shown in Fig. 8. It is clear in Fig. 8, *A* and *B*, that the annulus exerted a small but increasing excitatory effect as it encroached into the CRF, but one that was smaller than the plateau in the patch tuning curve (marked by the dashed line). These observations would be consistent with the predictions either for a suppressive field that surrounded the excitatory CRF or for those following from the difference of Gaussians model with overlapping inhibitory and excitatory fields.

However, for the majority of the cells in our sample (34/54, 63%), the largest response to an annulus was either not significantly different to (7/34 cells) or was significantly more than (27/34 cells) the plateau in the area summation curve ($P < 0.05$). Two examples are shown in Fig. 9. In both cases, the response to an annulus within the CRF substantially exceeded that to the plateau in the patch tuning curve (picked up by the dashed line) and indeed the response to the optimal patch diameter (picked up by the dotted line). Thus for both these cells, including the very center of the CRF in a stimulus that extended beyond the CRF reduced the response rather than enhanced it suggesting an increase in the magnitude of the "suppressive effect." Interestingly, the example in Fig. 9*A* shows that the response to the annulus decreased as it encroached further into the central region of the CRF. For these two examples, one could argue that the optimal stimulus was an annulus excluding the very center of the CRF. For the group as a whole, the mean best response to an annulus driving the CRF was 195 ± 68.10% larger than the response level for the plateau in the patch tuning curve. Taking each category of annulus encroachment into the CRF in turn, the responses for the outer 25% were 100 ± 82.53% larger, middle category 83 ± 25.21% larger, and inner category 85 ± 35.63% larger. It is clear for these cells that including the very center of the CRF in a stimulus extending beyond the borders of the CRF *reduced* the response rather than enhanced it. Thus for these cells, the surround suppressive mechanism appeared to be enhanced by, and in some cases require (as in Fig. 9), activation of the CRF center. This pattern of effect is neither simply predicted by the differences of Gaussians model or a surrounding inhibitory field.

To simplify the description, we refer to those cells showing annulus responses that were significantly below the plateau in the patch tuning curve as classical surround suppression (CSS) cells and the others as center gated surround suppression (CGSS) cells. The block histogram in Fig. 10*A* summarizes the differences in the mean relative response levels of the CSS and CGSS category cells to annuli in comparison to the plateau response from the patch tuning curve. The distinction between the two groups is further highlighted if one considers the response magnitudes with respect to the optimal. For the CSS category, the best annulus responses were 84 ± 3.22% smaller than the optimal while for the CGSS group the best annulus responses were only 34 ± 7.65% smaller than the optimal, as shown in Fig. 10*B*. We highlight the CSS and CGSS behavior because it underlines patterns of response that are sufficiently different to suggest distinct roles in the processing of the visual input. This point is underlined by the scatter diagram in Fig. 10*C* that plots the response to a large patch driving plateau-level response against the response to an annulus with the inner wall set at the diameter eliciting the best response. Cells with CSS properties are denoted by circles in the plot and those with CGSS properties by triangles. The dashed line identifies the diagonal denoting equal responses to annuli and large patches driving plateau-level responses. The broad distinction between the two categories is clear, although it remains open to question as to whether they reflect distinct groupings or two ends of a continuum deriving from a varying level implementation of the

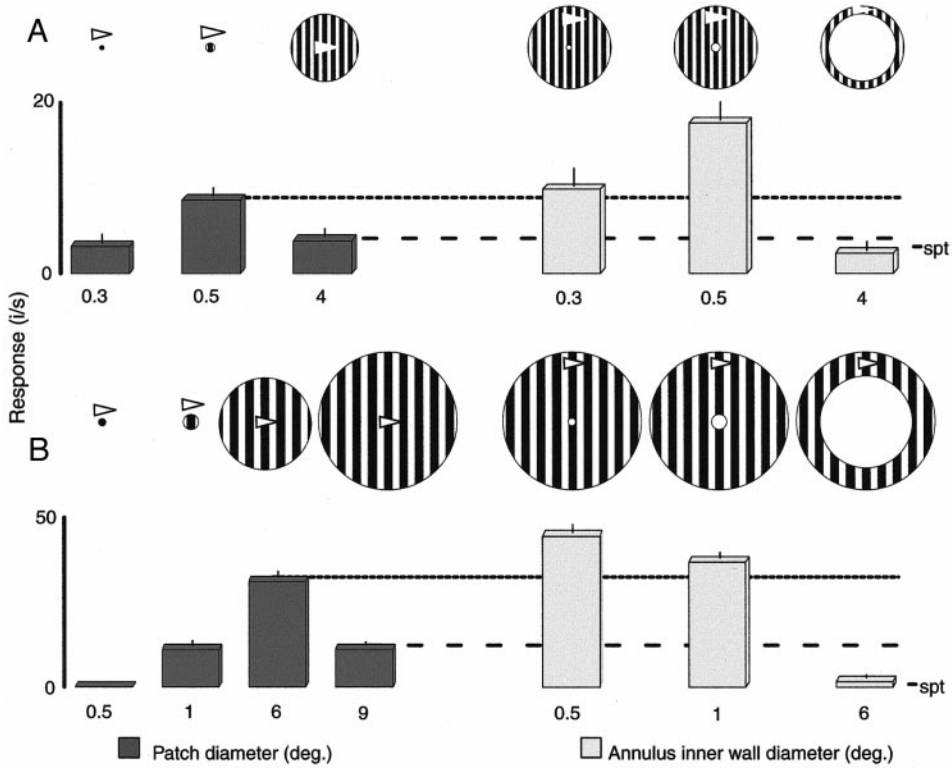

FIG. 9. Block histograms showing that excitatory response to an annulus falling within the CRF can exceed the responses to the plateau in the patch tuning curve. *A*: patch responses are denoted by the dark gray stippled bars to the *left* of the figure, annulus responses by the light gray stippled bars on the *right*. Stimulus configuration is denoted schematically *above* each bar. Patch and annulus inner wall diameters are indicated *below* each bar (0.3, 0.5, and 4°, respectively). The best response to an annulus exceeded the response seen in the patch tuning curve at the plateau (response level denoted by dashed line) and the optimal response in the patch tuning curve (dotted line). (24 stimulus repeats, SF, 2 c/d; TF, 3 Hz; contrast, 0.36. layer 4Cβ cell.) *B*: stimulus convention as for *A*. (Details as for *A*, but patch/annulus inner wall diameters are 0.5, 1, 6, and 9°. 50 stimulus repeats, SF, 1 cpd; Layer 6 cell.)

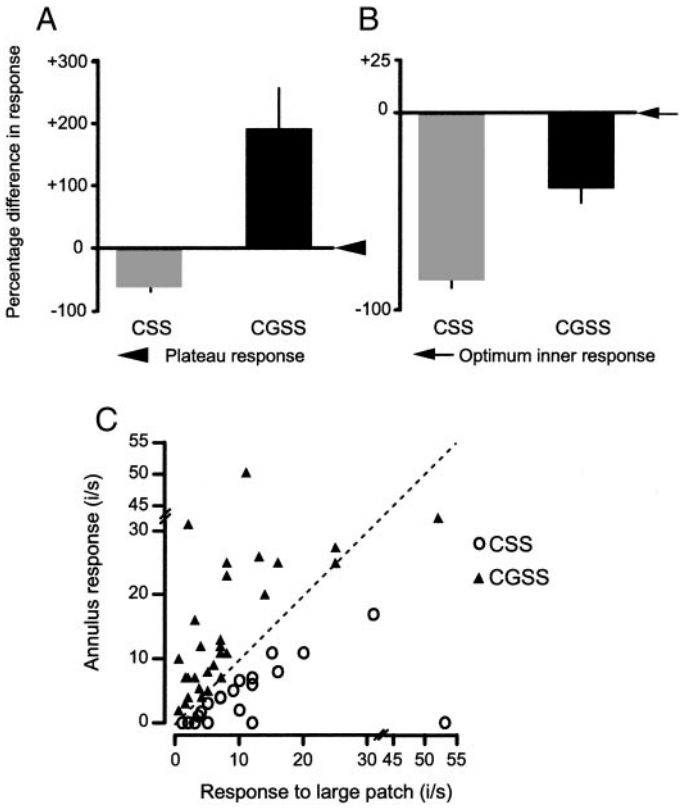

FIG. 10. *A* and *B*: block histograms summarizing the mean relative responses of our population of classical surround suppression (CSS) and center-gated surround suppression (CGSS) cells to annuli in comparison to the plateau response from the patch tuning curve (*A*) or the optimal response from the patch tuning curve (*B*). In *A*, the histogram plots the mean difference in response for the most effective annulus tested in comparison to the response level seen for the plateau of the patch tuning curve. The response at the plateau of the patch tuning curve (marked by the arrow head) is set to 0 so that negative values indicate that the response to the annulus was smaller than that at the plateau of the patch tuning curve, whereas positive values indicate that the responses were larger. CSS cells are denoted by the gray bar, CGSS cells by the black bar. Error bars indicate 1 SE. In *B*, the histogram plots the difference in response for the most effective annulus tested in comparison to the optimal inner patch response. The optimal patch response (marked by the arrow) is set to 0 so that negative values indicate that the response to the annulus was smaller than the optimal patch response. Bar conventions as in *A*. *C*: distribution of plateau vs. annulus responses for CSS and CGSS cell groups. The graph plots the response (in imp/s) to a large diameter patch along the *x* axis vs. the best response observed to an annulus along the *y* axis. CSS cells are denoted by circles and CGSS cells by triangles.

process generating the deviation of CGSS cell response from that which might be predicted from simpler mechanisms. The essential point though is that the two extremes encompass cells that, on the one hand, respond better to an annulus of drifting grating that excludes the center and, on the other, respond better to a patch of drifting grating that excludes the surround.

We were interested to ascertain whether we could isolate another measure of the distinction between these two groups. If the suppression derived from the surround, then the annulus response would be a mirror reflected image of the patch response. Assuming this to be the case, one can compute the number of excess spikes (if any) that an annulus produced over the prediction. We have thus computed the number of excess spikes produced by an annulus over the prediction based on the shape of the mirror-image patch-tuning curve (but resetting the prediction to 0 if the prediction was negative). This produced figures of 3.6 ± 0.69 (SE) imp/s for CSS cells and 11.7 ± 1.60 imp/s for CGSS cells. These values were statistically significantly different at the $P < 0.001$ level (Mann-Whitney *U* test). The difference was not because CGSS cells had a higher overall firing rate than CSS cells because the mean optimal firing rate for CSS cells was if anything slightly higher at 29 ± 5.00 imp/s than that for CGSS cells (25 ± 3.56 imp/s), although the differences were not statistically significant. We also quantified the number of excess spikes as a percentage of the optimal patch response. The mean value for CSS cells was 13.6 ± 2.48% and that for CGSS cells was 59.4 ± 6.56%. These values were statistically significantly different at the $P < 0.001$ level (Mann-Whitney *U* test). These figures show that both the CSS and CGSS cells drive extra spikes, but there seems to be a very robust enhancement of the effect in the transition to CGSS cells. Overall this supports the concept of a mechanism, potentially present across all cells in the sample but implemented with varying strength, to form two extrema in the pattern of responses to annuli.

Influence of direction of stimulus motion on surround suppression

It is clear from previous and current work in our laboratory (Sillito et al. 1995) and that of others (Born and Tootell 1991; Knierim and Van Essen 1992; Nothdurft et al. 1999) that surround suppression in primate V1 is generally tuned to the same orientation as a cell's excitatory response. Thus it is likely that the connections between cortical columns tuned to the same orientation (Bringuier et al. 1999; Gilbert and Wiesel 1989; Kisvárday and Eysel 1992; Malach et al. 1993; Ts'o and Gilbert 1988; Ts'o et al. 1986) must provide a significant contribution to the degree of surround suppression. However, this could be either via direct facilitatory inputs that might tend to decrease the degree of suppression or indirect connections via inhibitory interneurons that would enhance it. Additionally it is not clear whether the pattern of influence would be the same when the direction of the surround stimulus is reversed. Although effects have been described for a range of stimulus configurations involving motion contrast (Lamme 1995; Orban 1994; Orban et al. 1989), this has not been systematically examined in the context of the mechanisms underlying surround suppression in the primate. At least one reason for this is that the incidence and strength of surround suppression in primate V1 has not previously been appreciated. We thus examined the effect of reversing the direction of motion of the surround stimulus. These observations were made on 51 cells of our sample. All cells included in the analysis exhibited a PSI more than 20%. We examined the effect of reversing the direction of motion of the surround stimulus at range of different interface diameters for the center surround border. This was to enable us to examine the effect of reversing the direction of motion on surround suppression for a border within, on the edge of, and outside the CRF. We observed different types of effect from the reverse direction configuration. In the first instance, we have summarized these for the interface diameter generating the largest effect (where there was an effect of reversing the direction), and then we examine the influence of the location of the interface border with respect to the CRF.

For 22% of the cells tested (11/51), reversing the direction of drift of the surround had no effect on the magnitude of sup-

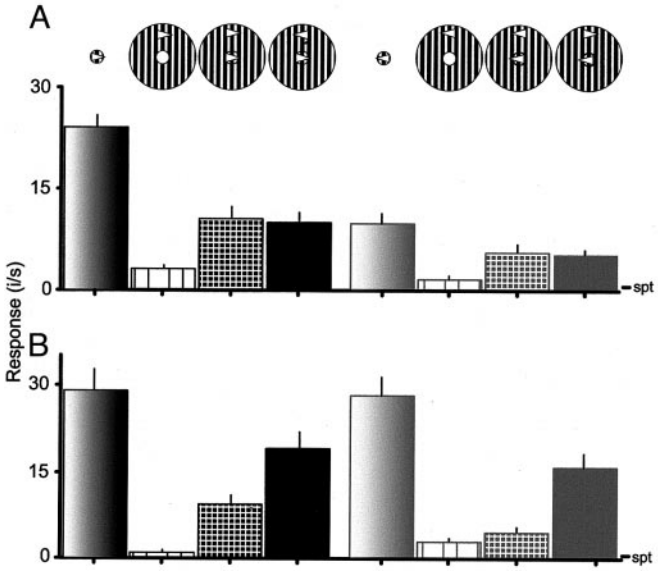

FIG. 11. These histograms document the responses of 2 V1 cells to a direction contrast stimulus. *A*: the 4 columns on the *left plot,* respectively, the response (in imp/s) to an inner patch of grating drifting in the cell's preferred direction of motion (*column 1*), the response to an annulus of grating drifting in the preferred direction (*column 2*) and then the response to the inner patch of grating drifting in the preferred direction presented simultaneously with the annulus of grating drifting in the same (*column 3*) or opposite (*column 4*) direction. The 4 columns to the *right plot* the response for the opposite direction of drift of the inner stimulus. Stimulus conditions are summarized schematically above each record. Error bars denote +1 SE. (Patch/interface diameter 1°. TF, 3 Hz; SF, 2 cpd; contrast, 0.36. 25 stimulus repeats. S type layer 4A cell.) *B*: convention as in *A.* (Patch/interface diameter, 0.75°. Further stimulus details as in *A,* but SF, 3 cpd; S type layer 4 B cell.)

pression at any interface diameter tested. For this subgroup, the mean suppression (with respect to the response to the inner stimulus alone) for the iso-direction surround was 45 ± 9.31% compared with a value of 49 ± 8.24% for the reverse direction surround. An example of the tests carried out on one of these cells is illustrated in Fig. 11*A*. The icons above the bar chart indicate the stimulus configurations. The cell exhibited directional selectivity to the inner stimulus alone but for either direction introducing an outer stimulus drifting in either the same or opposite direction reduced the response. For these cells, the mechanism driving the surround suppression would appear to integrate both directions of motion equally, even where, as for the example in Fig. 11*A*, the excitatory response driven from the field center was directionally selective. We should qualify our comments for this group with the comment that one of the cells showed a small, but just significant, increase in suppression when the direction of motion of the outer stimulus was reversed. This shift is included in the average change for the group quoted in the preceding text. These cells were thus not sensitive to direction contrast but were sensitive to the size of the stimulus.

The remaining cells were all sensitive to direction contrast, showing significant changes in surround suppression when the direction of drift of the outer was opposite to that of the inner. These cells fell into two groups, one showing a direction-contrast-dependent modulation of the strength of surround suppression and the other a direction-contrast-driven facilitation of responses. The group exhibiting direction-contrast modulation constituted 41% (21/51) of our sample and showed a reduction from a mean suppression of 70 ± 4.11% for the iso-direction surround to 22 ± 5.31% for the reverse direction surround, thus reflecting a partial but not total reduction in the strength of the surround suppression. An example of the responses of one of these cells is shown in Fig. 11*B*. The cell showed no directional selectivity to the inner stimulus, suppression when the outer stimulus moved in the same direction, and a reduction in surround suppression when the direction of the outer stimulus was reversed. This would seem to indicate that the mechanism integrating the suppression in these cells was only fully enabled when the surrounding and central area of visual space were engaged by the same direction of motion. Equally, a significant component of suppression (22%) remained in the reverse direction configuration, suggesting the possibility of two groups of lateral interactions driving the surround suppression.

Some of the complexities in the process generating suppression are underlined by the responses of the cells showing

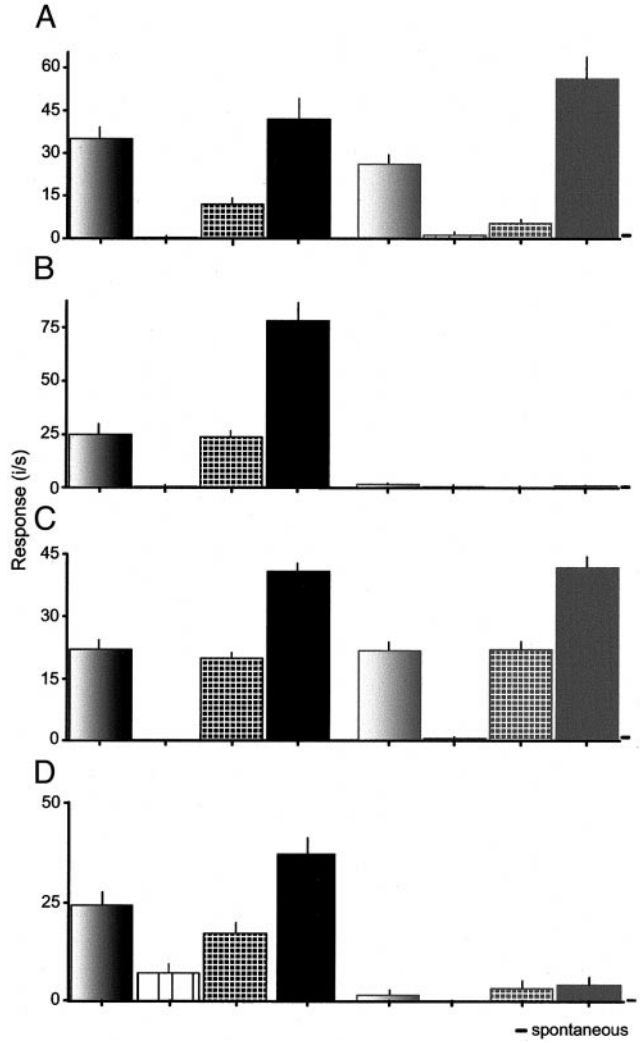

FIG. 12. Further examples of the effects of direction contrast between iso-oriented stimulus components. Conventions as for Fig. 11. *A*: patch/interface diameter 1°. TF, 3 Hz; SF, 2 cpd; contrast, 0.36. 15 stimulus repeats. C type layer 4B cell. *B*: further details as for Fig. 12*A*. S type layer 4B cell. *C*: further details as for Fig. 12*A* but patch/interface diameter 1.5°. S type layer 4Cα cell. *D*: further details as for Fig. 12*A* but 20 stimulus repeats. Patch/interface diameter was 1°. The 1° patch was the optimal single stimulus for this cell. C type layer 4B cell.

direction contrast facilitation. These constituted 37% (19/51) of our sample, and when the direction of the outer stimulus was opposite to that of the inner, their responses exceeded that to the inner alone. For these cells, the iso-direction surround stimulus elicited a suppression of 28 ± 5.79% of the response to the inner alone at the interface diameter used for the test, while the response in the presence of the reverse direction surround was a mean facilitation of 74 ± 15.69%. Examples of this pattern of response are given in Fig. 12, *A–C*. Note that in Fig. 12, *A–C*, the diameter of the central patch used for the tests was larger than the optimal diameter for a single patch. For each of these cells, although the reverse direction configuration evoked a response level higher than that to the inner stimulus used in the test, the responses did not exceed the response elicited by the optimal single stimulus. Thus the reverse direction enhancement may reflect a disinhibitory mechanism serving to reset the lower firing level associated with the particular inner stimulus toward the cell's optimal (see DISCUSSION and following text). In some cases, as in Fig. 12*D*, the response to the direction contrast configuration exceeded that evoked by the optimal single patch diameter stimulus. Of the cells showing direction-contrast facilitation, 26% (5/19) showed this "supra-optimal" facilitation. For this group in isolation, the mean response reduction associated with the iso-direction surround was 23 ± 14.67% at the interface diameter used for the test, while the mean response increase for the reverse direction configuration was 133 ± 45.87%. This translated into a mean increase of 95% above the value for the optimal diameter stimulus alone. The lower degree of iso-direction suppression reported here for the examples showing reverse direction facilitation and supra-optimal facilitation merely reflects the fact that many of these effects were only observed with interface diameters where the inner stimulus exceeded the CRF size (and was hence already driving a component of surround suppression, see following text). There was no significant difference ($P > 0.05$, Mann-Whitney U test) in the absolute degree of surround suppression derived from the area summation curves for the group of cells showing direction contrast facilitation and those that did not.

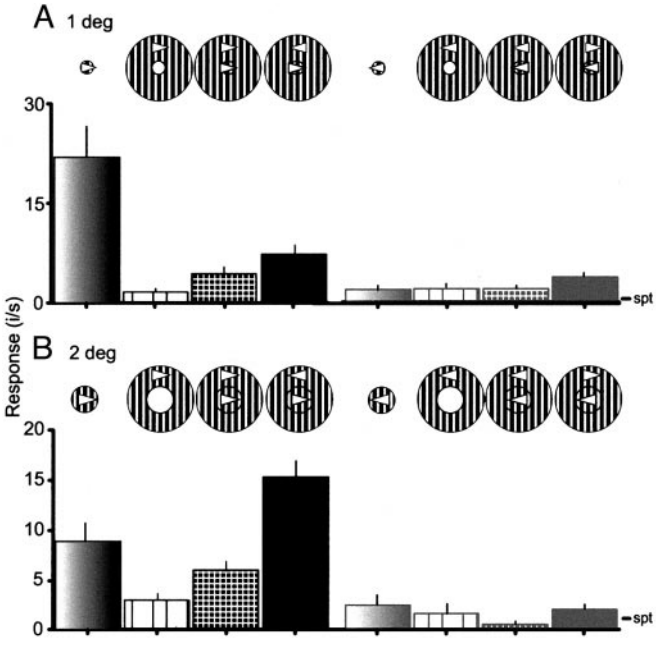

FIG. 13. Histograms show the effect of changing the patch/interface diameter on direction contrast effects for an S type cell recorded in layer 3. Conventions as for Fig. 11. *Top row*: the responses obtained with a patch/interface diameter of 1°; *bottom row*: the response of the cell to the same stimulus configuration but with the patch/interface diameter held at 2°. (Patch/interface diameter 1°. TF, 3 Hz; SF, 2 cpd; contrast, 0.36. 35 stimulus repeats.)

For the cells showing direction contrast facilitation, changing the interface diameter could change the response. An example is given in Fig. 13, *A* and *B*, where it is clear that adding a surround stimulus to a 1° inner stimulus (the optimal diameter for this cell) caused a strong suppression when it drifted in the same direction and a still clear but weaker suppression in the other direction. However, when the stimulus diameter was increased to 2°, although adding a surround drifting in the same direction again strongly suppressed the cell's response to the inner alone, reversing the direction of drift of the outer resulted in a response level exceeding that to the 2° inner alone. It is to be noted that the response level associated with the reverse direction configuration at 2° did not exceed that to the 1° inner (optimal diameter) alone, but the reverse direction configuration at 2° resulted in a response that was substantially larger than that to the reverse direction configuration at 1°. It is important to emphasize that none of the cells placed in the category exhibiting equal suppression to either direction of drift of the outer stimulus showed any other effect at any other diameter. Similarly none of the cells placed in the category showing direction contrast modulation of the level of surround suppression with direction of drift exhibited direction contrast facilitation at any stimulus interface diameter [and the majority exhibited similar effects at diameters smaller (57%) or larger (83%) than that showing the largest directionally dependent modulation]. For the cells showing direction contrast facilitation, 80% exhibited either equal effects or simple modulation of surround strength for the reverse direction configuration at smaller interface diameters than those revealing the largest facilitation and 89% at larger diameters.

The distribution of effects observed across our sample is summarized in the scatter diagram in Fig. 14*A* that compares the modulatory effect of a surround stimulus drifting in the same direction as the center stimulus (x axis) to that of a surround stimulus drifting in the opposite direction (y axis), on the response elicited by the center stimulus alone. Suppressive effects are denoted by negative values, response enhancements by positive values. In nearly all cases, the iso-direction surround stimulus reduced the response to the center stimulus alone so that virtually all points fall in the left two quadrants of the plot. Cells where both directions of the surround elicited equal suppressive effects, as shown in Fig. 11*A*, lie along the diagonal (◆). We have termed this group "no direction contrast effects." Less than a quarter of the cells tested showed this pattern of effect. The remaining cells all lie above the diagonal, indicating that an iso-direction surround elicited more suppression than a reverse direction surround. Cells such as that shown in Fig. 11*B*, where both drift directions of the surround stimulus suppress the center response, but where the suppressive effect elicited by the reverse direction surround is weaker, fall in the lower left quadrant, above the diagonal (□). We have termed this pattern of effect "direction contrast modulation." Cells such as those shown in Fig. 12, where the reverse direction stimulus enhances the response to the center stimulus lie in the upper left quadrant (○). We termed this pattern of

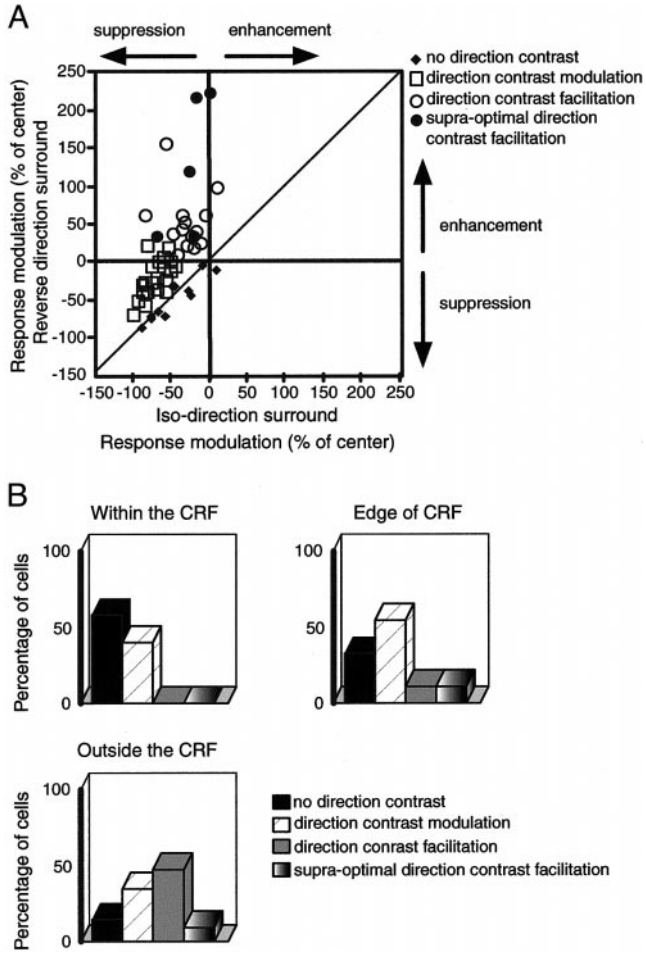

FIG. 14. *A*: comparison of the modulatory effects elicited by surround stimuli drifting in the same direction and in the opposite direction to the center stimulus on the response elicited by the center stimulus alone. The modulatory effect of the iso-direction surround stimulus is plotted along the *x* axis and that of the reverse-direction surround stimulus along the *y* axis. Suppressive effects are denoted by negative values, response enhancements by positive values. Cells where both directions of the surround elicited equal suppressive effects, as shown in Fig. 11*A*, lie along the diagonal (◆, no direction contrast cells). Cells where both drift directions of the surround stimulus suppress the center response but where the suppressive effect elicited by the reverse direction surround is weaker, fall in the lower left quadrant, above the diagonal (□, direction contrast modulation cells). Cells where the reverse direction stimulus enhances the response to the center stimulus lie in the upper left quadrant (○, direction contrast facilitation). Cells where the magnitude of the response observed to the reverse direction configuration exceeded the response elicited by the optimal single stimulus are marked by the ● (supra-optimal direction contrast facilitation). *B*: summary histograms documenting the prevalence of the various patterns of direction contrast effects with respect to whether the interface border between the inner and outer stimulus components was within, on the edge of, or outside the classical receptive field (CRF). The histogram for each location documents the proportion of cells tested at that location that exhibited each of the pattern of effects indicated by the keys to the right. See text for further details.

effect "direction contrast facilitation." For five cells, the magnitude of the response observed exceeded the response elicited by the optimal single stimulus (●) as illustrated in Fig. 12*D*. We have termed this effect "supra-optimal direction contrast facilitation."

We summarize the effect that the interface diameter between inner and outer stimuli had on the influence of the outer stimulus on the response to the inner stimulus in Fig. 14*B*. The results are grouped for interface diameters within, on the edge of, and outside the CRF. The height of the columns indicates the percentage of cells showing each of the four patterns of effect described in the preceding text (no direction contrast, direction contrast modulation, direction contrast facilitation, and supra-optimal direction contrast facilitation) for the three groups of interface diameter. The supra-optimal group are represented both as part of the facilitatory group and again as a separate subset. The main conclusion from this is that reverse direction configuration facilitatory effects (inclusive of the supra-optimal group) were seen predominantly for interface diameters larger than the CRF, although some were seen on the edge of the CRF. However, none were observed for interface diameters within the CRF. Simple reductions in suppression for direction contrast were seen at all three groups of interface diameter. The fact that most of the direction contrast facilitatory effects were observed for interface diameters larger than the CRF suggests that the effect requires the central component of the stimulus to be driving the surround suppression mechanism. It argues for the possibility that the reverse direction facilitatory effect may involve disinhibition (see preceding text). Thus the "facilitation" reflected an increase back toward the value associated with a smaller diameter stimulus optimally driving the cell. We speculate that the cells showing "supra-optimal facilitation" may reflect cases where the degree of suppression implemented within the CRF was stronger (see DISCUSSION) and so the influence of disinhibition was greater.

In Fig. 15, we show the laminar distribution of cells in the different groups of effect characterized in these experiments. Those showing no direction contrast effects were only seen in lamina 2–4Cα, whereas those showing a reduction in the level of suppression to direction contrast were seen through all laminae. The cells showing direction contrast facilitation were

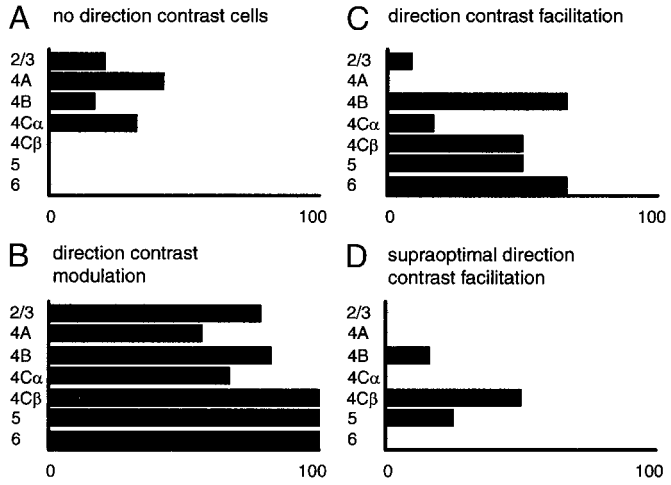

FIG. 15. Comparison of the laminar distribution of the various patterns of direction contrast effects across our sample of V1 cells. Each histogram plots the proportion of cells recorded in each lamina showing the pattern of effect noted *above*, expressed as a percentage of the total number of cells recorded in each lamina. *A*: histogram plots the proportion of cells recorded in each lamina that showed no direction contrast modulation, expressed as a percentage of the total number of cells recorded in each lamina. *B*: histogram plots the proportion of cells showing direction contrast effects and includes cells showing direction contrast modulation of suppression, direction contrast facilitation and direction contrast supra-optimal facilitation. *C*: histogram plots the proportion of cells showing direction contrast facilitation (including those that showed supra-optimal direction contrast modulation). *D*: histogram plots the proportion of cells showing supra-optimal direction contrast facilitation.

mainly seen in layers 4B-6 and those showing supra-optimal facilitation in layers 4B, 4Cβ, and 5. It is interesting that the modulation of surround suppression by direction was seen through all layers while the cells showing directional specificity (absolute preference for one direction of motion) or directional selectivity (the response to the preferred direction was more than 200% more than the response to the nonpreferred direction) to a single stimulus had a restricted laminar distribution, being primarily located in layers 4B and 6, broadly comparable with previous reports in the literature (Hawken et al. 1988; Orban et al. 1986).

The previous characterization of the location of effects with respect to the CRF borders (see Fig. 14*B*) of course integrates the influence from all location around the CRF. To dissect the localization of areas that might drive the direction contrast effects, we examined the distribution of locations driving reverse direction effects with the duo patch paradigm shown in Fig. 6. In Fig. 16, *A–C*, we compare for three of the examples shown in Fig. 6 the effect of reversing the direction of drift of the outer patch. For the cell shown in Fig. 16*A*, there is simply a loss of the inhibitory zones that were characterized by the iso-direction patch while that in Fig. 16*B* retains an area of mild suppression to one side of the field. In contradistinction, the cell in Fig. 16*C* showed both a loss of the suppressive areas and the appearance of facilitatory regions at the outer margins of the area tested with a particularly potent effect from one corner. In each case, the center patch dimensions equate to the CRF size. A further example in Fig. 16, *D* and *E*, shows tests carried out on a cell with patches of, respectively, 1 and 2° diameter. In this case, the 1° patch corresponded to the size of the CRF. For the smaller diameter patches, this cell showed suppression from all locations around the field with a bias to the upper end of the zone surrounding the central stimulus. Interestingly the strength of this was increased when the direction of motion of the second patch was reversed and the suppression was uniformly distributed around the CRF. With the 2° patches, a different pattern emerged. The second patch evoked a strong suppression from the lower end of the zone surrounding the central stimulus in the iso-direction of motion and strong facilitatory effects from the flanks when the direction of motion was reversed. This underlines the impact of the size of both the stimuli overlying the CRF and those outside the CRF on the pattern of response and shows the complexity of effects that may contribute to the pattern seen with the concentric stimuli of varying dimensions.

We quantified the degree and pattern of spatial heterogeneity for the direction contrast facilitation using the same methodology based on circular statistics (Batschelet 1981) described in the preceding text. However, in this case, the term *Fi* representing the magnitude of the facilitatory effects observed at each location replaced the term *Si* in each equation. *Fi*, the magnitude of facilitation (expressed as a percentage of the

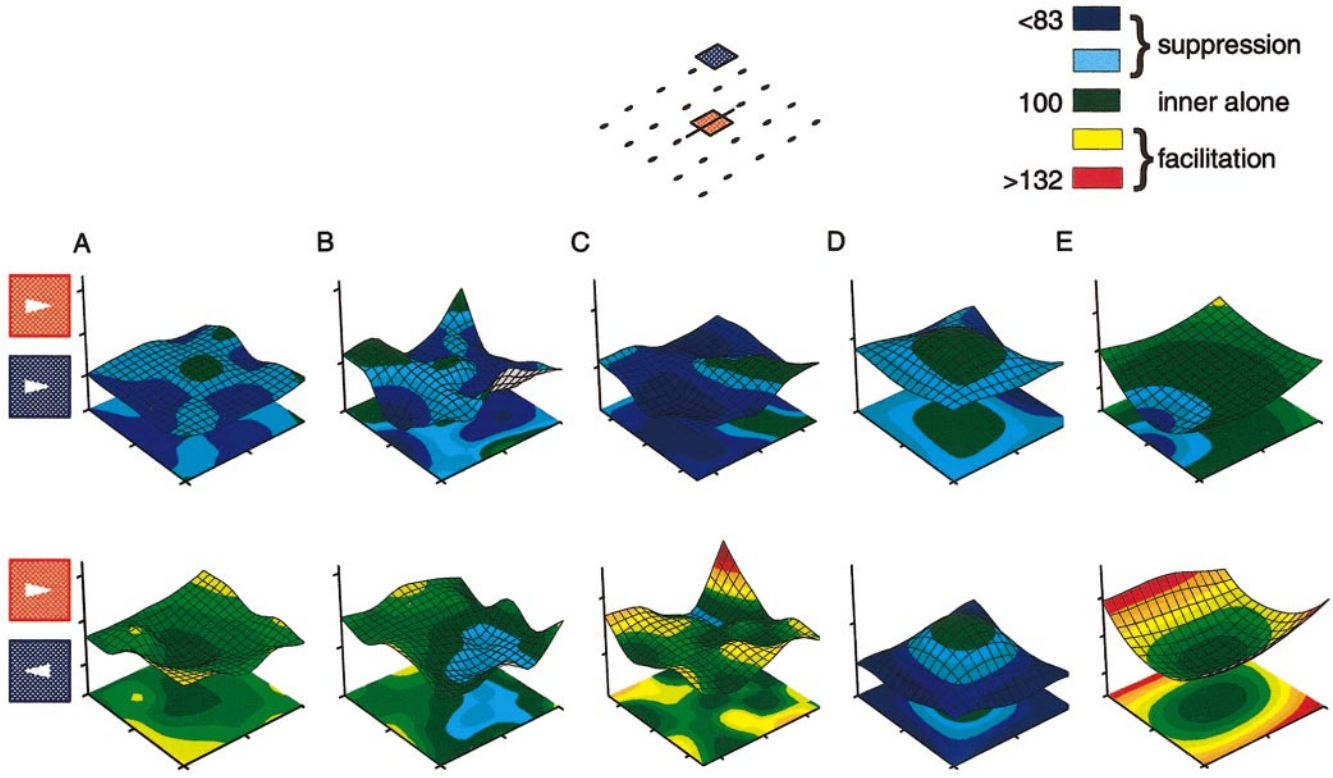

FIG. 16. The surface plots depict the modulatory effects of iso-direction and reverse direction surround stimuli positioned at a number of locations, on the response to a central patch. The stimulus configuration comprised an inner stimulus (a square patch centered over the CRF containing an optimally oriented grating drifting in the cell's preferred direction of motion) and a 2nd stimulus (another square patch of optimally oriented grating) which was positioned at a range of *xy* locations around the central stimulus (as depicted by the schematic diagram *above*) and which was drifted in either the same direction of motion as the center patch (*top*) or the opposite direction (*bottom*). In each plot, the responses are normalized with respect to the response elicited by the center patch alone (100% in each case, dark green). Suppressive effects are denoted by blue colors, facilitatory effects by light green to red colors (see color scale bar *top right*). See text for further details. Center patch diameter ranged from 1 to 2° depending on each cell's CRF size. Spatial frequency ranged from 2 to 3 cpd. Temporal frequency, 3 Hz. Contrast 0.36.

response to the center stimulus alone) for each surround stimulus location, was computed according to the formula $F = [(R_{cs}/R_c) - 1]*100$, where R_{cs} is the response to the combination of the center and surround stimulus and R_c is the response to the center stimulus presented alone. We used the same statistical criteria to subdivide cells into three groups, those exhibiting spatially uniform surround facilitation, spatially asymmetric surround facilitation and bilaterally symmetric surround facilitation. Again, the majority of cells (89%) exhibited spatial heterogeneity of surround locations with only 11% of cells showing spatially uniform surround facilitation. Both spatially asymmetric facilitatory effects where the surround facilitation was concentrated in one location (33%) and bilaterally symmetric facilitatory effects were observed (56%). Direction contrast facilitation was obtained from the ends, sides, and corners of the visual space surrounding the CRF, and there was no evidence to suggest that the mechanisms underlying the effect were concentrated in either end-zone or sideband regions.

DISCUSSION

These data underline the prevalence and strength of surround suppression in primate V1, reinforcing and extending the observations made in earlier reports (Sceniak et al. 1999; Sillito et al. 1995). In addition, they show a complexity to the patterns of spatial organization associated with surround suppression that invoke comparison with work on surround mechanisms in area MT (Raiguel et al. 1995; Xiao et al. 1995, 1997b). It is clear from our work that suppressive surround effects do not necessarily simply follow from end zones or side bands and that a wide range of patterns of spatial organization can apply with many showing asymmetric patterns. Moreover the strength and nature of the effects varied with the size of the stimuli used. In particular, we would highlight the fact that for the majority of cells reversing the direction of motion of a stimulus in the surround strongly modulated its influence with, in more than a third of the cells, suppressive effects being replaced by facilitatory effects. This strong influence of motion contrast, together with the heterogeneity in the spatial organization of the surrounds, again aligns the organization in V1 with properties described in MT (Allman et al. 1985; Lagae et al. 1989; Raiguel et al. 1995; Tanaka et al. 1986; Xiao et al. 1995, 1997b). It suggests that there is an organization already implemented in V1, or following from the feedback from MT, that provides a substrate for complex operations such as the extraction of information about three-dimensional structure from motion gradients (Xiao et al. 1997a,b). One might suggest that there is a case for considering some facets of the V1 organization as being very similar to MT but simply scaled down.

It is important not to lose sight of the simple observation regarding the strength of surround suppression for the contrast used here (0.36) when a stimulus is extended uniformly beyond the borders of the CRF. We observed that 94% of the cells in our sample ($n = 105$) exhibited on average a 67% reduction in output below the level seen with the same stimulus parameters spatially restricted to the CRF. Moreover, more than 40% of our sample showed a more than 70% reduction in response levels when the stimulus extended beyond the CRF. These effects were observed to be distributed through all laminae, and the range of effects was similar in all laminae, suggesting that the mechanism was common to the circuitry in V1. This is the first report that clearly links magnitude of suppression and laminar distribution in primate V1, although there is a reference linking suppression to superficial layer cells (Born and Tootell 1991). Another study described surround suppressive effects from static texture patterns composed of line elements (Nothdurft et al. 1999), but the overall magnitude of the suppression for these was lower than that reported here. This may follow from differences in the pattern of the process engaged by the static line patterns. The prevalence and strength of the suppressive effect reported here is very important because, given the minute size of the CRF of primate V1 cells, it underlines the massive response reduction in the network underlying the retinotopic representation associated with quite small patches of coherent oriented moving stimuli even for the relatively low contrast we used (cf. Vanduffel et al. 2000).

A further interesting facet of the observations on the suppression is the fact that we observed a substantive variation in the response of cells to uniform surround stimuli leading to the identification of two patterns of behavior embedded in our sample. The distinction between the two patterns was revealed by the use of an annulus of drifting grating in which the diameter of the inner wall was varied so that we studied the effect of a stimulus encroaching on the field from the surround rather than expanding out of the field from the center. As an annulus by definition excludes the receptive field center, but encompasses all the surround, one would predict the best response to an annulus to be less than the plateau in the area summation curve. In line with this, we observed that one group of cells (37%) either failed to respond to the annulus as it progressively encroached onto the CRF or exhibited a response that was less than the plateau in the spatial summation curve for a circular patch of increasing diameter. This behavior is essentially what would be predicted from either the difference of Gaussian's model or a surrounding suppressive field. We called these classical surround suppression cells (CSS). The other cells (63%) were characterized by the fact they exhibited responses to an annulus that were either equal to or more than those of the plateau in the summation curve for a circular patch of drifting grating. In this sense, these cells encompassed responses that are not explained by the difference of Gaussians model. These we called center-gated surround suppression cells (CGSS). The significant point here is that for the CGSS cells a stimulus that extended substantially beyond the CRF but excluded the very center could drive them very effectively while for the CSS group such a stimulus produced little if any response. In both cases, a stimulus restricted to the center of the CRF was highly effective, although in some cases in the CGSS group, activation of the excitatory mechanism from the surround (but excluding the very center of the field) evoked a larger excitatory response than any diameter of stimulus overlying the CRF. Thus in the extremes, there were cells that gave their best responses to a stimulus that excluded the center while there were others that only responded to a stimulus that excluded their surround (from those that were 100% patch suppressed).

Our analysis suggests that the mechanism underlying the response of the CGSS cells might be reflected across the entire sample but implemented to a higher level in the CGSS cells. The behavior of CGSS cells in the area summation test fol-

lowed what would be predicted from for example the difference of Gaussians model. It deviated from this when tested with a stimulus that excluded the center but encompassed the surround. We speculate that the essential characteristics of the receptive field of both CSS and CGSS cells involves overlying excitatory and inhibitory fields as encapsulated in the difference of Gaussians model. Additionally, however, we propose that the process expressed in CGSS cells includes a laterally driven facilitatory influence from adjacent columns that when stimulated by an annulus excluding the field center but activating the surround, tips the balance in favor of the excitatory mechanism in the field. When, on the other hand, the center of the CRF of these cells is driven, it activates a reciprocal lateral inhibitory process that suppresses those surrounding cells generating the facilitatory input leaving the balance of the core mechanisms as seen in CSS cells. The final caveat is that this additional mechanism may exist in all cells but vary in the magnitude of its expression.

It is important to stress that the strong surround suppression observed here with stimuli extending uniformly beyond the receptive field center should not be considered to be incompatible with the facilitatory effects reported when line elements or Gabor patches are added in a sequence along an axis parallel to a cell's optimal orientation (Ito and Gilbert 1999; Kapadia et al. 1995; Polat et al. 1998). It is clear that variations in the spatial extent and contrast of stimuli (Jagadeesh and Ferster 1990; Kapadia et al. 1999; Sceniak et al. 1999) can engage the excitatory and inhibitory mechanisms in different ways (see also models by Dragoi and Sur 2000; Somers et al. 1998). Many lines of evidence (Bringuier et al. 1999; Gilbert and Wiesel 1989; Kisvárday and Eysel 1992; Malach et al. 1993; Ts'o et al. 1986, 1988) suggest that there are excitatory links between columns of similar orientation selectivity and that these must provide a basis for facilitatory interactions between line elements of similar orientation. The outcome must be seen as a balance between the extent to which the stimuli engage inhibitory interactions which mask the influence of the excitatory connections.

The effect of reversing the direction of motion of the surround stimulus underlines the subtle nature of the balance of effects contributing to surround suppression. For some cells (22%), predominantly in the superficial laminae, the direction of drift of the outer stimulus had no effect on the degree of suppression, suggesting an integration of processes driven from both directions of motion in the mechanism generating the suppression. For the remainder though, the reverse direction configuration either reduced the degree of suppression (37%) or turned the suppression into a facilitatory effect (41%). For the cells showing just a reduction in the suppression, this could be seen to reflect the possibility that some of the lateral connections mediating surround effects were themselves directionally selective (but not all because some suppression remained), i.e., they linked cells in iso-orientation columns with the same directional selectivity. However, we would underline the point that sensitivity to direction contrast was seen in cells through all layers and in cells which were not themselves directionally selective. The virtual absence of cells in our data showing enhanced suppression when the direction of the stimulus was reversed contrasts with reports made for cat V1 (Gulyás et al. 1987; Sengpiel et al. 1997; Walker et al. 1999). This together with the lower level of suppression seen in cat V1 (Jones et al. 2000; Sengpiel et al. 1997; Toth et al. 1996; Walker et al. 1999) suggests an area of difference in the functional organization. It is also worth noting that examples such as the cell illustrated in Fig. 16, *D* and *E*, where one size of the duo patch stimuli used to dissect the surround effects revealed reverse direction enhancement of suppression and the larger size reverse direction facilitation, indicate the way several contrasting mechanisms can be embedded in the surround mechanism. The nature of the stimulus used determines what is seen.

The facilitatory effects to direction contrast configurations suggest that more complex interactions may pertain. These were only observed for interface diameters on the edge of or outside the CRF. In particular, they were associated with diameters of the inner stimulus that were more than the optimal and thus the inner stimulus alone was driving mechanisms pushing the response below optimal rates. From this perspective, they could be argued to reflect a disinhibitory process reducing the gain or space constant of the mechanism generating the inhibitory input. The supra-optimal facilitatory effects might follow from a more potent version of the same interaction. One simple suggestion is that processes driven by the same direction of motion reinforce the inhibitory mechanism influencing both its gain and space constant and that reversing the direction of the outer stimulus reduces this and exposes facilitatory inputs both within the CRF and from laterally displaced iso-orientation columns responding to the reverse direction. In this sense, there could also be a shift in the gain and space constant of the excitatory mechanism (Sceniak et al. 1999) enabled by the reverse direction excitatory inputs. The fact that the facilitatory effects were only drawn from direction contrast interfaces at or beyond the border of the CRF implies a dynamically structured implementation of connections between directionally selective mechanisms in hypercolumns drawing on adjacent areas of visual space. Where the direction contrast border fell within the CRF, facilitatory effects were not obtained, although reductions in suppression were seen, despite the fact that the outer stimulus would clearly engage the laterally directed interactions that subserved the facilitatory effects when the border was outside the CRF. This implies that the CRF border as defined here, marks a point where there is a transition in the way laterally directed interactions are enabled. We should also not ignore the influence of feedback from MT raised at the beginning of this discussion. As the scale of the stimuli increase it may be that feedback from MT is more effectively driven and this could serve to change the gain and balance of the elements of the circuitry in V1 or exert direct facilitatory effects for example.

The change in pattern of effect with the spatial scale of the stimuli, whether concentric or duo patch, suggests a phasing of the connections mediating different categories of influence with distance from the CRF center. It also seems that the extent of the stimulus overlying the CRF may induce effects that enable different patterns of convergence from the areas of the network driven by the surround. This may be reciprocal and could involve influences that are mediated by lateral interactions within the network of interactions in V1 and by reflected lateral interactions deriving from higher level feedback (e.g., MT). It is pertinent to consider the fact that V1 cells are often studied with elongated contours such as bars and that the results of dissection with these stimuli emphasize flanking

sidebands and end zones. There are several points to make here. The first is that the visual world is not generally composed of single bar stimuli. The second is that circuitry in V1 is a highly interconnected network and that, as the present study underlines, different classes of stimuli will invoke different patterns of spatial convergence on the cell. In this sense, neither the CRF nor any other facet of the behavior determined by particular classes of stimuli can be regarded as an invariant description of some absolute property of the cell. They are merely a description of the cell's and, more cogently the network's, behavior under a certain class of stimulus conditions. We suggest that the nature of the surround is dynamically determined by the interplay and spatial scale of the specific configurations of stimuli driving the system. Depending on contrast, the common default can be suppression for stimuli that extend uniformly beyond the CRF with a declining effectiveness as this contrast falls with the consequence that the underlying excitatory input is increasingly exposed. Equally, more complex stimuli engage the local circuitry and feedback in different ways and enable convergent interactions that subserve the processes necessary to optimize the extraction of information for the type of image driving the system.

We are indebted to D. Matin for skilled technical assistance and Dr. Zhaoping Li for comments on the manuscript.

The support of the Medical Research Council is gratefully acknowledged.

REFERENCES

AHMED B, ANDERSON JC, DOUGLAS RJ, MARTIN KAC, AND NELSON JC. Polyneuronal innervation of spiny stellate neurons in cat visual cortex. *J Comp Neurol* 341: 39–49, 1994.

ALLMAN JM, MIEZIN F, AND MCGUINNESS E. Direction- and velocity-specific responses from beyond the classical receptive field in the middle temporal area (MT). *Perception* 14: 105–126, 1985.

BATSCHELET E. *Circular Statistics in Biology*. London, UK: Academic, 1981.

BRINGUIER V, CHAVANE F, GLAESER L, AND FREGNAC Y. Horizontal propagation of visual activity in the synaptic integration field of area 17 neurons. *Science* 283: 695–699, 1999.

BORN RT AND TOOTELL RBH. Single-unit and 2-deoxyglucose studies of side inhibition in macaque striate cortex. *Proc Natl Acad Sci USA* 88: 7071–7075, 1991.

CALLAWAY EM. Local circuits in primary visual cortex of the macaque monkey. *Annu Rev Neurosci* 21: 47–74, 1998.

DEANGELIS GC, FREEMAN RD, AND OHZAWA I. Length and width tuning of neurons in the cat's primary visual cortex. *J Neurophysiol* 71: 347–374, 1994.

DRAGOI V AND SUR M. Dynamic properties of recurrent inhibition in primary visual cortex: contrast and orientation dependence of contextual effects. *J Neurophysiol* 83: 1019–1030, 2000.

FERSTER D AND LINDSTROM S. Augmenting responses evoked in area 17 of the cat by intracortical axon collaterals of cortico-geniculate cells. *J Physiol (Lond)* 367: 217–232, 1985a.

FERSTER D AND LINDSTROM S. Synaptic excitation of neurones in area 17 of the cat by intracortical axon collaterals of cortico-geniculate cells. *J Physiol (Lond)* 367: 233–252, 1985b.

GILBERT CD AND WIESEL TN. Columnar specificity of intrinsic horizontal and corticocortical connections in cat visual cortex. *J Neurosci* 9: 2432–2442, 1989.

GULYÁS B, ORBAN GA, DUYSENS J, AND MAES H. The suppressive influence of moving textured backgrounds on responses of cat striate neurons to moving bars. *J Neurophysiol* 57: 1767–1791, 1987.

HAWKEN MJ, PARKER AJ, AND LUND JS. Laminar organization and contrast sensitivity of direction-selective cells in the striate cortex of the Old World monkey. *J Neurosci* 8: 3541–3548, 1988.

HUBEL DH AND WIESEL TN. Receptive fields binocular interaction and functional architecture in the cat's visual cortex. *J Physiol (Lond)* 160: 106–154, 1962.

HUBEL DH AND WIESEL TN. Receptive fields and functional architecture in two nonstriate visual areas (18 and 19) of the cat. *J Neurophysiol* 28: 229–289, 1965.

ITO M AND GILBERT CD. Attention modulates contextual influences in the primary visual cortex of alert monkeys. *Neuron* 22: 593–604, 1999.

JAGADEESH B AND FERSTER D. Receptive field lengths in cat striate cortex can increase with decreasing stimulus contrast. *Soc Neurosci Abstr* 16: 130.11, 1990.

JONES HE, ANDOLINA IM, OAKELY NM, MURPHY PC, AND SILLITO AM. Spatial summation in lateral geniculate nucleus and visual cortex. *Exp Brain Res* 135: 279–284, 2000.

KAPADIA MK, ITO M, GILBERT CD, AND WESTHEIMER G. Improvement in visual sensitivity by changes in local context: parallel studies in human observers and in V1 of alert monkeys. *Neuron* 15: 843–856, 1995.

KAPADIA MK, WESTHEIMER G, AND GILBERT CD. Dynamics of spatial summation in primary visual cortex of alert monkeys. *Proc Natl Acad Sci USA* 96: 12073–12078, 1999.

KATO H, BISHOP PO, AND ORBAN GA. Hypercomplex and simple/complex cell classifications in cat striate cortex. *J Neurophysiol* 14: 1071–1095, 1978.

KISVÁRDAY ZF AND EYSEL UT. Cellular organization of reciprocal patchy networks in layer III of cat visual cortex (area 17). *Neuroscience* 46: 275–286, 1992.

KNIERIM JJ AND VAN ESSEN DC. Neuronal responses to static texture patterns in area V1 of the alert macaque monkey. *J Neurophysiol* 67: 961–980, 1992.

LAGAE L, GULYÁS B, RAIGUEL S, AND ORBAN GA. Laminar analysis of motion information processing in macaque V5. *Brain Res* 496: 361–367, 1989.

LAMME VAF. The neurophysiology of figure-ground segregation in primary visual cortex. *J Neurosci* 15: 1605–1615, 1995.

LUND JS. Anatomical organization of Macaque monkey striate visual cortex. *Annu Rev Neurosci* 11: 253–288, 1988.

MALACH R, AMIR Y, HAREL M, AND GRINVALD A. Relationship between intrinsic connections and functional architecture revealed by optical imaging and *in vivo* targeted biocytin injections in primate striate cortex. *Proc Natl Acad Sci USA* 90: 10469–10473, 1993.

MERRILL EG AND AINSWORTH A. Glass-coated platinum-plated tungsten microelectrodes. *Med Biol Eng Comp* 10: 662–672, 1972.

NOTHDURFT HC, GALLANT JL, AND VAN ESSEN DC. Response modulation by texture surround in primate area V1: correlates of popout under anaesthesia. *Vis Neurosci* 16: 15–34, 1999.

ORBAN GA. Motion processing in monkey striate cortex. In: *Cereb Cortex* 10: 413–441, 1994.

ORBAN GA, KATO H, AND BISHOP PO. End-zone region in receptive fields of hypercomplex and other striate neurons in the cat. *J Neurophysiol* 42: 818–832, 1979a.

ORBAN GA, KATO H, AND BISHOP PO. Dimensions and properties of end-zone inhibitory areas in receptive fields of hypercomplex cells in cat striate cortex. *J Neurophysiol* 42: 833–849, 1979b.

ORBAN GA, KENNEDY H, AND BULLIER J. Velocity sensitivity and direction selectivity of neurons in areas Vl and V2 of the monkey: influence of eccentricity. *J Neurophysiol* 56: 462–480, 1986.

ORBAN GA, LAGAE L, RAIGUEL S, GULYÁS B, AND MAES H. Analysis of complex motion signals in the brain of cats and monkeys. In: *Models of Brain Function*, edited by Cotterill RMJ. London: Cambridge, 1989, p. 151–165.

PETERS A, PAYNE BR, AND BUDD J. A numerical analysis of the geniculocortical input to striate cortex in the monkey. *Cereb Cortex* 4: 215–229, 1994.

POLAT U, MIZOBE K, PETTET MW, KASAMATSU T, AND NORCIA AM. Collinear stimuli regulate visual responses depending on cell's contrast threshold. *Nature* 391: 580–584, 1998.

RAIGUEL S, VAN HULLE MM, XIAO DK, MARCAR VL, AND ORBAN GA. Shape and spatial distribution of receptive fields and antagonistic motion surrounds in the middle temporal area (V5) of the macaque. *Eur J Neurosci* 7: 2064–2082, 1995.

RODIECK RW. Quantitative analysis of cat retinal ganglion cell response to visual stimuli. *Vision Res* 5: 583–601, 1965.

ROSE D. Responses of single units in cat visual cortex to moving bars of light as a function of bar length. *J Physiol (Lond)* 271: 1–23, 1977.

SCENIAK MP, RINGACH DL, HAWKEN MJ, AND SHAPLEY R. Contrast's effect on spatial summation by macaque V1 neurons. *Nat Neurosci* 2: 733–739, 1999.

SENGPIEL F, SEN A, AND BLAKEMORE C. Characteristics of surround inhibition in cat area 17. *Exp Brain Res* 116: 216–228, 1997.

SILLITO AM, CUDEIRO J, AND MURPHY PC. Orientation sensitive elements in the corticofugal influence on centre-surround interactions in the dorsal lateral geniculate nucleus. *Exp Brain Res* 93: 6–16, 1993.

SILLITO AM, GRIEVE KL, JONES HE, CUDEIRO J, AND DAVIS J. Visual cortical mechanisms detecting focal orientation discontinuities. *Nature* 378: 492–496, 1995.

SKOTTUN BC, DE VALOIS RL, GROSOF DH, MOVSHON JA, ALBRECHT DG, AND BONDS AB. Classifying simple and complex cells on the basis of response modulation. *Vision Res* 31: 1079–1086, 1991.

SOMERS DC, TODOROV EV, SIAPAS AG, TOTH LJ, KIM DS, AND SUR M. A local circuit approach to understanding integration of long-range inputs in primary visual cortex. *Cereb Cortex* 8: 204–217, 1998.

STRATFORD KJ, TARCZY-HORNOCH K, MARTIN KAC, BANNISTER NJ, AND JACK JJB. Excitatory synaptic inputs to spiny stellate cells in cat visual cortex. *Nature* 382: 258–261, 1996.

TANAKA K, HIKOSAKA K, SAITO H, YUKIE M, FUKADA Y, AND IWAI E. Analysis of local and wide-field movements in the superior temporal visual areas of the macaque monkey. *J Neurosci* 6: 134–144, 1986.

TOTH LJ, RAO SC, KIM DS, SOMERS D, AND SUR M. Subthreshold facilitation and suppression in primary visual cortex revealed by intrinsic signal imaging. *Proc Natl Acad Sci USA* 93: 9869–9874, 1996.

TS'O DY AND GILBERT CD. The organization of chromatic and spatial interactions in the primate striate cortex. *J Neurosci* 8: 1712–1727, 1988.

TS'O DY, GILBERT CD, AND WIESEL TN. Relationships between horizontal interactions and functional architecture in cat striate cortex as revealed by cross-correlation analysis. *J Neurosci* 6: 1160–1170, 1986.

VANDUFFEL W, TOOTELL RBH, AND ORBAN GA. Attention-dependent suppression of metabolic activity in the early stages of the macaque visual system. *Cereb Cortex* 10: 109–126, 2000.

WALKER GA, OHZAWA I, AND FREEMAN RD. Asymmetric suppression outside the classical receptive field of the visual cortex. *J Neurosci* 19: 10536–10553, 1999.

WALKER GA, OHZAWA I, AND FREEMAN RD. Suppression outside the cortical classical receptive field. *Visual Neurosci* 17: 369–379, 2000.

XIAO DK, MARCAR VL, RAIGUEL SE, AND ORBAN GA. Selectivity of macaque MT/V5 neurons for surface orientation in depth specified by motion. *Eur J Neurosci* 9: 956–964, 1997a.

XIAO DK, RAIGUEL S, MARCAR V, KOENDERINK J, AND ORBAN GA. Spatial heterogeneity of inhibitory surrounds in the middle temporal visual area. *Proc Natl Acad Sci USA* 92: 11303–11306, 1995.

XIAO DK, RAIGUEL S, MARCAR V, AND ORBAN GA. Spatial distribution of the antagonistic surround of MT/V5 neurons. *Cereb Cortex* 7: 662–677, 1997b.